CALIFORNIA INSTITUTE OF TECHNOLOGY

EARTHQUAKE ENGINEERING RESEARCH LABORATORY

# CHARACTERIZING AVERAGE PROPERTIES OF SOUTHERN CALIFORNIA GROUND MOTION AMPLITUDES AND ENVELOPES

BY

GEORGIA CUA AND THOMAS H. HEATON

REPORT NO. EERL 2009-05

PASADENA, CALIFORNIA

FEBRUARY 2008

A REPORT ON RESEARCH SUPPORTED BY THE CALIFORNIA INSTITUTE OF TECHNOLOGY UNDER THE SUPERVISION OF THOMAS HEATON.

**Characterizing average properties of southern California ground motion amplitudes and envelopes**

Georgia Cua[1] and Thomas H. Heaton[2]

[1]Swiss Seismological Service, ETH Zurich, Switzerland

[2]California Institute of Technology

**Abstract**

We examine ground motion envelopes of horizontal and vertical acceleration, velocity, and filtered displacement recorded within 200 km from southern California earthquakes in the magnitude range $2 < M \leq 7.3$. We introduce a parameterization that decomposes the observed ground motion envelope into P-wavetrain, S-wavetrain, and ambient noise envelopes. The shape of the body wave envelopes as a function of time is further parameterized by a rise time, a duration, a constant amplitude, and 2 coda decay parameters. Each observed ground motion envelope can thus be described by 11 envelope parameters. We fit this parameterization to 30,000 observed ground motion time histories, and develop attenuation relationships describing the magnitude, distance, and site dependence of these 11 envelope parameters. We use these relationships to study 1) magnitude-dependent saturation of peak amplitudes on rock and soil sites for peak ground acceleration, peak ground velocity, and peak filtered displacement, 2) magnitude and distance scaling of P- and S-waves, and 3) the reduction of uncertainty in predicted ground motions due to the application of site-specific station corrections. We develop extended magnitude range attenuation relationships for PGA and PGV valid over the magnitude range $2 < M < 8$ by supplementing our dataset of S-wave envelope amplitudes with the Next Generation Attenuation (NGA) strong motion dataset. We compare extended magnitude range attenuation relationships with the Campbell and Bozorgnia (2008) and Boore and Atkinson (2008) NGA relationships. Our extended magnitude range attenuation relationships exhibit a stronger inter-dependence between distance and magnitude scaling. This character of ground motion scaling becomes evident when

examining ground motion amplitudes over an extended magnitude range, but is not apparent when considering data within a more limited magnitude range, for instance, the *M>5* range typically considered for strong motion attenuation relationships.

## Introduction

The widespread deployment of seismic stations in southern California under the TriNet project resulted in an unprecedented dataset of recorded ground motions (Mori et al., 1998). We analyzed a large portion of this dataset as part of a study on seismic early warning (Cua, 2005). We studied envelopes of ground motion, as opposed to the fully sampled time histories, due to our interests in developing a seismic early warning methodology for deployment on the Southern California Seismic Network (SCNS); peak ground motion information (acceleration, velocity, and displacement) over 1-second window lengths are among the data packets that arrive in closest to real-time at the central processing facility of the SCSN. In this study, we define ground motion envelopes as the peak ground motion value over non-overlapping one-second windows; this definition is consistent with the type of data streams that can be realistically produced by seismic networks in real-time.

We developed a parameterization that decomposed the observed ground motion envelope time history into P-wavetrain, S-wavetrain, and ambient noise envelopes. Each wavetrain envelope is described by a rise time, a peak amplitude, a duration, and two coda decay parameters. We analyzed 9 components of ground motion: 2 horizontal and 1 vertical component of acceleration, velocity, and filtered displacement. With this parameterization, the evolution of each component of ground motion amplitude as a function of time is described by 11 envelope parameters (5 P-wave parameters, 5 S-wave parameters, and 1 constant to describe ambient noise levels). We use the neighborhood algorithm, a nonlinear direct search algorithm (Sambridge, 1999a, 1999b) to find the set of 11 maximum likelihood envelope parameters for each envelope wavetrain in the database.

We developed attenuation relationships that describe each of these 11 envelope parameters as a function of magnitude, distance, site condition, component, and type of ground motion parameter (acceleration, velocity, displacement). In this paper, we focus the discussion on the attenuation relationships for peak P- and S-wave amplitudes of horizontal and vertical ground motion acceleration, velocity, and filtered displacement on rock and soil sites. We use these attenuation relationships to study 1) magnitude-dependent saturation of peak amplitudes on rock and soil sites, 2) magnitude and distance scaling of P- and S-waves, and 3) the reduction of uncertainty in predicted ground motions due to the application of site-specific station corrections.

The fact that the TriNet project provides well calibrated broad-band motions over a very large amplitude range allows us the opportunity to study the interdependence of magnitude scaling and distance scaling for acceleration, velocity, and displacement. In previous studies that consider only strong motions from large earthquakes, the magnitude range is small enough that empirical prediction equations that consist of independent distance decay terms and magnitude scaling terms can approximately capture trend in the data (Boore and Atkinson, 2008; Campbell and Bozorgnia, 2008). However, using a data set with a much larger range of magnitudes, we find compelling evidence that amplitude decay with distance and magnitude scaling cannot be separated. For example, we find that near-source peak accelerations change their magnitude scaling from $10^{\frac{3}{2}M}$ for small magnitudes to complete saturation at large magnitudes. In contrast, peak near-source displacements change their magnitude scaling from $10^{\frac{3}{2}M}$ for small magnitudes to $10^{\frac{1}{2}M}$ for large magnitudes.

Since the data set in our study is large, we can derive separate prediction equations for rock and soil sites. We attribute differences in the prediction equations (except for an amplification factor) to nonlinear behavior of soil sites. In particular, we find that near-source peak accelerations from small earthquakes are about twice as large at soil sites than at rock sites, whereas near-source peak accelerations from large earthquakes are approximately the same for soil sites and rock sites. This behavior is consistent with yielding of soil sites at large amplitudes that serves to nonlinearly increase effective damping for soil sites. We also find that P-wave amplitudes appear to exhibit stronger saturation characteristics than S-wave amplitudes, particularly in the horizontal direction.

In this study we also use the Next Generation Attenuation (NGA) strong motion dataset (http://peer.berkeley.edu/nga) to supplement our southern California data set to derive extended magnitude range attenuation relationships for peak ground acceleration (PGA) and peak ground velocity (PGV) valid up to 200 km epicentral distance over the magnitude range $2 < M < 8$. We compare the median ground motion levels predicted by our extended magnitude range relationships with those predicted by the Boore and

Atkinson (2008) and Campbell and Bozorgnia (2008) relationships developed as part of the NGA project.

The NGA relationships, and the majority of attenuation relationships in the literature, are used in seismic hazard analyses to provide estimates of either the median, geometric mean, or random component of the horizontal ground motions. However, none of these are representative of the maximum ground motion level experienced by a given building during an earthquake, which is the vector amplitude of the horizontal ground motions. We also develop conversion factors between the vector amplitude of horizontal ground motion with other commonly used measures of horizontal ground motion.

## Method

### Waveform dataset

Waveforms for this study were obtained from 1) the Southern California Earthquake Center (SCEC) database (http://www.data.scec.org) which archives waveform data recorded by the Southern California Seismic Network (SCSN), and 2) the Consortium of Organizations for Strong Motion Observation Systems (COSMOS) database (http://db.cosmos-eq.org), which archives strong motion data from the U.S. Geological Survey, California Geological Survey, and other strong motion arrays worldwide. Many SCSN stations have co-located broadband and strong motion instruments, and contribute 3 components of broad-band seismometer records (for small to moderate motions) and 3 components of accelerometer records (for moderate to large motions). We typically used the broadband velocity waveforms. However, if we found evidence of clipping (visual examination, or peak velocities exceeding 13 cm/s, the typical clip level of an STS-2 seismometer), then we downloaded the strong-motion accelerometer data instead.

We performed gain and baseline corrections on the downloaded waveforms and integrated and/or differentiated to obtain acceleration, velocity, and displacement time histories. The displacement waveforms were filtered using a 3-second, 4-pole high-pass Butterworth filter to reduce the influence of microseisms on small amplitude displacements. This filter also removes long-period noise introduced in the processing of strong motion records.

We examined ground motions recorded at 150 Southern California Seismic Network (SCSN) stations located within 200 km epicentral distance of 70 Southern California events in the magnitude range $2 < M \leq 7.3$. In addition to SCSN data, we also included strong motion records from the COSMOS database from the 1989 $M=7.0$ Loma Prieta, 1991 $M=5.8$ Sierra Madre, 1992 $M=7.3$ Landers, 1992 $M=6.4$ Big Bear, and 1994 $M=6.7$ Northridge (and a $M=5.1$ aftershock) earthquakes. Ground motion envelopes time series were obtained from the 100- or 80-sample per second time series by taking the maximum amplitudes over one-second non-overlapping windows.

**Site classification**

We adopted a binary (rock-soil) site classification based on the southern California site classification map of Wills et al (2000), which was based on correlating the average shear wave velocity in the upper 30 m (Vs30) with geologic units. Wills et al (2000) created intermediate categories BC and CD to accommodate geologic units that had Vs30 values near the boundaries of the existing NEHRP-UBC site classes. In our binary site classification, "rock" sites are those assigned to classes BC and above (Vs30 > 464 m/s), and "soil" sites are those with classification C and below (Vs30 ≤ 464 m/s). Of the SCSN stations we used, 35 stations were classified as rock, and 129 stations were classified as soil stations. Separate attenuation relationships for the various envelope parameters were developed for rock and soil sites, allowing us to investigate differences in the average properties of ground motions on rock and soil sites over the magnitude and distance ranges covered by our dataset. Since SCSN stations, which are almost all located on rock or stiff soil sites, contribute the majority of the ground motions in our dataset, this study does not include records from very soft soils (E class, or Bay mud-type sites).

**Next Generation Attenuation (NGA) strong motion dataset**

The S-wave envelope amplitude for horizontal acceleration or velocity for a given record is equivalent to the maximum acceleration or velocity observed on a given channel. We can relate these envelope amplitudes to peak ground acceleration (PGA) and peak ground velocity (PGV), which are fundamental quantities of interest in seismic hazard analyses. When deriving attenuation relationships for these particular envelope parameters, we supplement the southern California S-wave envelope amplitudes with amplitudes from a subset of the NGA strong motion database used by Boore and Atkinson (2008). We will refer to this subset of the NGA database as the NGA dataset for brevity. The NGA dataset contributes 50 additional records to the rock category, and 1557 additional records to the soil category. The largest event from the NGA dataset is the 2000 $M = 7.9$ Denali, Alaska earthquake. It should be emphasized that general analysis of the waveform envelopes and the associated envelope parameters uses the southern California dataset. The NGA dataset is used as a supplement only for the attenuation of the S-wave envelope amplitudes for horizontal acceleration (PGA) and velocity (PGV).

Figure 1 shows the distribution in magnitude and distance space of the data (southern California envelope dataset and NGA strong motion dataset) used in this study. Each point on these plots for the southern California dataset contributes waveforms for 9 channels of ground motion (vertical, North-South, and East-West components for each of acceleration, velocity, and filtered displacement). For each channel of ground motion, there are 958 records from rock sites, and 2,630 records from soil sites.

**Parameterization of ground motion envelopes**

We modeled the observed ground motion envelopes as a combination of P-wavetrain, S-wavetrain, and ambient noise envelopes. The P-wavetrain, S-wavetrain, and ambient noise envelopes of a given record combine according to the rule:

$$E_{obs}(t) = \sqrt{E_P^2(t) + E_S^2(t) + E_{ambient}^2} + \varepsilon(t) \quad (1)$$

where $E_{obs}(t)$ is the observed ground motion envelope, $E_P(t)$, $E_S(t)$, $E_{ambient}$ are the modeled P-wavetrain, S-wavetrain, and ambient noise envelopes, and $\varepsilon(t)$ is the difference between the observed and modeled envelope.

The ambient noise envelope for a given time history, $E_{ambient}$, is modeled as a constant. The time dependence of the P- and S-wavetrain envelopes, $E_P(t)$ and $E_S(t)$, is piece-wise linear with Omori-type decay. Each of $E_P(t)$ and $E_S(t)$ is described by a rise time (*tr*), constant amplitude (*A*) with an associated duration ($\Delta t$), and two decay parameters ($\tau$, $\gamma$). We found that using a single decay parameter would typically fit the overall coda, but with large misfits immediately after the peak P- or S-wave amplitudes. Jennings et al (1968) also require two parameters to describe the decay of envelope amplitudes following the peak ground motion. Using two decay parameters improves the fit between the modeled and observed envelopes at the cost of introducing trade-offs in the parameterization.

$$E_{ij}(t) = \begin{cases} 0 & for\ t < T_i \\ \dfrac{A_{ij}}{tr_{ij}}(t - T_i) & for\ T_i \le t < T_i + tr_{ij} \\ A_{ij} & for\ T_i + tr_{ij} \le t < T_i + tr_{ij} + \Delta t_{ij} \\ \dfrac{A_{ij}}{(t - T_i - tr_{ij} - \Delta t_{ij} + \tau_{ij})^{\gamma_{ij}}} & for\ t \ge T_i + tr_{ij} + \Delta t_{ij} \end{cases}$$

*where*

$i =$ P-, S-wave

$T_i =$ P-, S-wave arrival times

$$j = \begin{matrix} \ddot{u}_Z, & \ddot{u}_{N-S}, & \ddot{u}_{E-W} \\ \dot{u}_Z, & \dot{u}_{N-S}, & \dot{u}_{E-W} \\ u_Z, & u_{N-S}, & u_{E-W} \end{matrix} \quad (2)$$

*with*

$\ddot{u}$ denoting acceleration

$\dot{u}$ denoting velocity

$u$ denoting displacement

A total of 11 envelope parameters (5 each for the P- and S-wave envelopes, and a constant for the ambient noise) are used to describe a single observed ground motion envelope.

The parameterization described by Eqns.(1) and (2) allows for a separate characterization for P- and S-wavetrains. It makes intuitive sense that each of the body wave envelopes has a rise time, an amplitude with a finite duration, and parameters describing its coda decay. Unfortunately, this intuitive parameterization is quite non-linear, due to trade-offs between the various parameters. For instance, we identified strong trade-offs between rise time and duration, and between the coda decay parameters $\tau$ and $\gamma$ for both P- and S-wave envelopes. Additional difficulties arose in uniquely characterizing the P-wave coda decay at close distances (less than 20 km), when there is less than 3 seconds of P-wave data before the onset of the S-wave arrival. Our aim was to quantify the time-dependence of the shape of ground motions envelopes on magnitude, distance, frequency band, and site condition.

In principle, we could postulate how the various envelope parameters depend on magnitude, distance, and site, and along with Eqn.(2), find the model parameters that best fit all envelope time histories in our database in a single very large and highly nonlinear inversion (Figure 2a). Instead, we use an iterative approach where the single large and nonlinear inverse problem is replaced by numerous small nonlinear inverse problems (Figure 2b). In this iterative approach, we use the neighborhood algorithm (NA) (Sambridge, 1999a, 1999b) to find the set of 11 envelope parameters that minimize $\varepsilon$ in Eqn.(1) in a least squares sense for each observed envelope time history in our dataset. Figure 3a shows the ground motion acceleration recorded at SCSN station Domenegoni Reservoir (DGR) during the 1994 M=6.7 Northridge earthquake. Figure 3b shows its ground motion envelope and the 11 least squares envelope parameters from the NA inversion. The set of envelope parameters carried to the next stage of the analysis for each given observed envelope time series was not necessarily the only good solution for that particular time series. There were families of “good” solutions in the neighboring regions of the parameters space, due to the trade-offs between the rise time and duration parameters, as well as between the two coda decay parameters. Fortunately, the P- and S-wave envelope amplitude parameters from the NA inversions were robust relative to these trade-offs.

Typically, each station has 1 vertical and 2 horizontal (from 2 orthogonally oriented horizontal sensors) time series available. These were differentiated and/or integrated to yield 9 waveforms for each station (1 vertical and 2 horizontal channels for each of acceleration, velocity, and filtered displacement). For each station, the NA was applied to all 9 waveforms. For each ground motion component (acceleration, velocity, and filtered displacement) at each station, the 2 sets of horizontal envelope parameters (from 2 orthogonally oriented sensors) were combined in a root mean square sense to define a single set of horizontal envelope parameters. Separate regressions were developed for 6 channels (1 each of vertical and horizontal acceleration, velocity, and filtered displacement) channels of envelope parameters.

## Envelope attenuation relationships for magnitude and distance

### Rise time, duration, and decay parameters

We modeled the logarithm of rise time (*tr*), logarithm of durations (*Δt*), and coda decay parameters (*τ,γ*) as linear functions of magnitude, distance, and log distance.

$$\begin{aligned} &\log(env\_param_{ij}) = \alpha_{ij} M + \beta_{ij} R + \delta_{ij} \log R + \mu_{ij} \\ &where\ \ env\_param_{ij} = \{tr_{ij}, \Delta t_{ij}, \tau_{ij}, \gamma_{ij}\} \end{aligned} \tag{3}$$

where subscripts *i*, *j* are as in Eqn.(2). The least squares model coefficients for these parameters are listed Tables 2.1-2.4. These Tables can also be downloaded from Appendix C of Cua (2005), http://resolver.caltech.edu/CaltechETD:etd-02092005-125601.

**P- and S-wave envelope parameters**

Of the 11 envelope parameters, the P- and S-wave amplitudes were expected to have the strongest magnitude and distance dependence. We used Eqn.(4) to model the magnitude, distance, and site dependence of P- and S-wave amplitudes for the 6 channels of ground motion.

$$
\begin{aligned}
&\log Y_{ijk} = a_i M_k + b_i (R_{1k} + C_{ik}(M_k)) + d_i \log(R_{1k} + C_{ik}(M_k)) + e_{ij} + \varepsilon_{ijk} \\
&\textit{where} \\
&i = 1,\ldots,24 \ \text{ (P-, S-wave amplitudes on rock and soil sites for 6 channels)} \\
&j = 1,\ldots, \ \text{number of stations} \\
&k = 1,\ldots, \ \text{number of records} \\
&Y_{ijk} = \ \text{body wave amplitude from NA algorithm inversion on given record} \\
&M_k = \ \text{reported magnitude (moment magnitude for } M > 5) \\
&R_k = \ \text{epicentral distance for } M < 5, \ \text{fault distance for } M \geq 5 \\
&R_{1k} = \sqrt{R_k^2 + 9} \ \text{ (assuming an average depth of 3 km for southern California events)} \\
&C_{ik}(M) = c_{1i} \exp(c_{2i}(M_k - 5)) \times \left(\arctan(M - 5) + \tfrac{\pi}{2}\right) \\
&e_{ij} = e_{1i} + e_{2ij} \ \text{ (constant term plus station-specific corrections)} \\
&\varepsilon_i = \ \text{statistical or prediction error,} \ \sim NID(0, \sigma_i^2)
\end{aligned}
\tag{4}
$$

For the ground motions at a given station, the horizontal body wave amplitudes are the root mean squares of the respective body wave envelope amplitudes from the 2 (orthogonal) horizontal records. Base-10 logs are used throughout this paper. In a later section of this paper, we derive factors that can be used to convert different measures of horizontal ground motion (for instance, geometric mean, larger random component, root mean square) to the maximum vector amplitude of the horizontal ground motions, which corresponds to the maximum ground motions amplitude experienced at a given site for a given earthquake.

Eqn.(4) has strong influences from traditional strong motion attenuation relationships, in particular, from the work of Boore and Joyner (1982), Boore, Joyner, and Fumal (1997) , and Campbell (1981; 2004). In the subsequent discussion, the subscripts *i,j,k* are dropped for brevity. The physical motivations for the various terms are as enumerated in the early literature on ground motion attenuation:

- $\log Y \propto aM$ is consistent with the definition of magnitude as the logarithm of ground motion amplitude (Richter, 1935)
- $\log Y \propto \log R^{-d}$ is consistent with the geometric attenuation of the seismic wavefront away from the source
- $\log Y \propto bR$ is consistent with anaelastic attenuation due to material damping and scattering
- $\log Y \propto e$ , where e is partitioned into a constant and station-specific site correction terms, is consistent with the multiplicative nature of site effects
- $C(M) = c_1 \exp(c_2(M-5)) \times \left(\arctan(M-5) + \frac{\pi}{2}\right)$ is a magnitude-dependent saturation term that allows ground motion amplitudes at close distances to large earthquakes (*M>5*) to be relatively independent of magnitude. Ground motion simulations suggest that the shape of attenuation curves is magnitude-dependent, with ground motion amplitudes in the near-source region of large earthquakes approaching a limiting value (Hadley and Helmberger, 1980). Campbell (1981)

found empirical evidence for such saturation in near-source peak accelerations from a dataset of near-source records (within 50 km) from global earthquakes with $M>5$. Since our southern California envelope dataset spans a larger magnitude range ($2 < M \leq 7.3$), we modify Campbell's original saturation term $C(M) = c_1 \exp(c_2 M)$ with an $\arctan(M-5) + \frac{\pi}{2}$ term to "turn on" saturation effects when $M>5$, while allowing the logarithm of ground motion amplitudes to scale linearly with magnitude for $M<5$. In our regressions, $c_2$ was constrained to be approximately 1, while $c_1$ varied depending on the degree of saturation exhibited by the data. Values of $c_1$ close to 0 mean no saturation, with increasing values of $c_1$ indicating stronger saturation effects. $C(M)$ has units of distance, and increasing $C(M)$ increases the "effective epicentral distance" of a given station.

The saturation function $C_i(M)$ makes Eqn.(4) a nonlinear function of the unknown model parameters ($a, b, c_1, c_2, d, e_1, e_{2ij}$). Note that we keep the subscripting on $e_{2ij}$ to emphasize that each channel has a unique set of station-correction terms. The model parameters are determined in a two-step process for each of the $i$, $(i=1,\ldots 24)$ regression analyses. In the first step, we use the neighborhood algorithm to find the set of model parameters ($a, b, c_1, c_2, d, e_1$) that minimize the residual sum of squares ($RSS$) between the observed amplitudes and those predicted by Eqn.(4). These model parameters are listed in Table 2.

$$RSS = \sum_{k=1}^{n} \left( \log Y_{obs} - \log Y(a,b,c_1,c_2,d,e_1) \right)^2 \qquad (5)$$

In Eqn.(5), $Y_{obs}$ are the set P- or S-wave amplitudes ($A_P$ or $A_S$) obtained from the NA inversions on individual records for all records in the database. In the second step, the station corrections, $e_{2ij}$ , are obtained by averaging the residuals between model predictions and the observations available at a given station. For each of the $i$ channels, the standard error of regression, $\sigma$, is a measure of how well the model fits the observations, and is given by

$$\sigma = \sqrt{\frac{RSS}{ndof}} \tag{6}$$

where $ndof$ denotes the number of degrees of freedom, which equals the number of available observations, $n$, less the number of model parameters determined via regression. Without station corrections, our regressions have $ndof=n-6$; with station corrections, $ndof=n-6-(number\ of\ stations)$. Station corrections were calculated only if 3 or more recordings from different earthquakes were available at a given station.

## Horizontal S-wave envelope amplitude for acceleration and velocity and the NGA relationships

Our horizontal S-wave envelope amplitudes for acceleration and velocity can be expected to correspond to peak ground acceleration (PGA) and peak ground velocity (PGV). There is a vast body of literature in strong motion attenuation studies describing the dependence of PGA, PGV, and peak response spectral quantities on various predictor variables (magnitude, distance, site condition, depth to basement, focal mechanism, tectonic setting, etc.) for $M>5$ events. The latest set of attenuation relationships for regions with shallow crustal seismicity is being developed by the Next Generation of

Ground Motion Attenuation project (the “NGA project”). The NGA project is a research initiative conducted by the Pacific Earthquake Engineering Research (PEER) center and the US Geological Survey, with the objective of developing updated empirical ground motion models for shallow crustal earthquakes (Power et al., 2008). Five developer teams are involved to provide a range of interpretations: Abrahamson and Silva, Boore and Atkinson, Campbell and Bozorgnia, Chiou and Youngs, and Idriss. Each developer team used the strong motion database compiled by the PEER-NGA project (NGA flatfile), and could choose whether to use the entire database, or selected subsets of the database. These five teams have authored a significant percentage of the existing literature on strong motion attenuation.

Typically, strong ground motion relationships are valid for $M>5$, with the primary application of predicting peak ground motions given a set of source and site characteristics for use in seismic hazard analysis and building design. However, with the increasing interest in earthquake early warning systems and ShakeMaps, which are most useful for the infrequent large events, but must be tested on the more frequent smaller events, there is a growing need to characterize ground motions from $M<5$ events. The most commonly used weak-motion relationship is the small-amplitude regression used by the USGS ShakeMap codes (Wald et al., 1999; 2005), which is valid for $M<5.3$. Thus far, there are no relationships that characterize both weak and strong motion scaling simultaneously.

We developed relationships for PGA and PGV spanning the magnitude range $2 < M < 8$ by fitting Eqn.(4) to a dataset consisting of our southern California horizontal S-wave envelope amplitudes ($A_S$) and the subset of the NGA dataset used by Boore and Atkinson (2008). These extended magnitude range attenuation relationships simultaneously fit weak and strong ground motion data with a single regression equation (Eqn.4). We compare our extended magnitude range attenuation relationships with the ShakeMap small amplitude weak-motion relationship and the Boore and Atkinson (2008) and Campbell and Bozorgnia (2008) NGA strong motion relationships. A comprehensive comparison of the 5 NGA relationships is beyond the scope of this study.

*Horizontal component definition*

There are numerous ways to combine 2 horizontal channels into a single characteristic measure of horizontal ground motion. NGA database lists the “GMRotI50” of the two horizontal components. “GMRotI50” is orientation-independent measure proposed by Boore et al (2006). Beyer and Bommer (2006) tabulated commonly used definitions in the literature, and derived conversion factors between these definitions and the geometric mean of the as-recorded motions, which we will refer to in this paper as the geometric mean. They found the ratio between GMRotI50 and the geometric mean of the 2 horizontal channels to be approximately 1. (Boore et al (2006) find the difference between GMRotI measures and the geometric mean to be less than 3%.) For the southern California envelope study, we used the root mean square to combine envelope parameters from the 2 horizontal channels. For the extended magnitude range PGA and PGV analysis, we used the geometric means of the as-recorded components for the southern

California weak motion data and GMRotI50 values of the NGA strong motion dataset. From Beyer and Bommer (2006), we can assume that these measures are approximately equivalent.

*Distance metric*

For the distance metric in our combined weak/strong motion relationships, we used the Joyner-Boore distance ($R_{jb}$), which is the closest distance to the surface projection of the fault. $R_{jb}$ is tabulated for records in the NGA database. For a large portion of our southern California $M<5$ events, $R_{jb}$ was not available, and we used epicentral distance.

## Results

We have 2 primary sets of results: 1) a set of envelope attenuation relationships derived from southern California waveforms, that can predict the shape of ground motion envelopes as a function of time for horizontal and vertical acceleration, velocity, and filtered displacement (given a magnitude, distance, and Vs30 or NEHRP site classification), and 2) extended magnitude range attenuation relationships for horizontal PGA and PGV derived from southern California S-wave envelope amplitudes ($2 < M \leq 7.3$) and the NGA strong motion dataset ($5 \leq M < 8$).

*Envelope attenuation relationships*

The envelope parameterization adopted (Eqn.(2)) is a point source characterization, and is valid up to M6.5. Figure 4 shows the average horizontal acceleration envelope on rock and soil sites at a variety of magnitude and distance ranges. At larger magnitudes, the relationships for envelope rise time, duration, and decay parameters (Tables 2.1-2.4) no longer hold. However, the relationships for envelope amplitudes ($A_P$, $A_S$) are still valid (Table 1). Larger events require finite source characterization. A possible approach to taking into account finite source characteristics is to use multiple point sources. Yamada et al (2007) utilize the point source envelope characterization developed in this study in their multiple-point source characterization of finite ruptures for large earthquakes.

*Magnitude, distance, frequency band, and site-dependence of P- and S-wave amplitudes*

The model coefficients for the magnitude and distance dependence of the P- and S-wave envelope amplitudes are listed in Table 1. Table 3 lists the model coefficients for PGA and PGV on rock and soil sites for the combined weak and strong motion relationships. When predicting horizontal S-wave acceleration and velocity amplitudes, we recommend using the coefficients listed in Table 3 (constrained by the NGA strong motion dataset) in place of the horizontal S-wave acceleration and velocity coefficients listed in Table 1 (which are constrained by the southern California dataset, which has limited data for $M>5$ events).

Figures 5 and 6 show the distance-dependence at various magnitudes levels of PGA and PGV attenuation relationships derived from the combined weak and strong motion datasets on both rock and soil sites. The soil site regressions are based on significantly more data than the rock site relationships. The symbols are the observed amplitudes from which the model was derived. Saturation effects come into play at close distances to $M>5$ events.

Figure 7 shows the residuals, (Eqn.(5)), for horizontal S-wave and P-wave acceleration amplitudes on rock sites as a function of magnitude and distance. The S-wave residuals are from the combined southern California and NGA dataset. The P-wave analysis uses only the southern California data. In these plots, the solid line corresponds to a residual value of 0. The dashed lines correspond to the 95% confidence intervals, $\pm 2\sigma$. There are no systematic trends in the residuals with either magnitude or distance. These residual plots are characteristic of the P- and S-wave residuals of the other amplitude regressions.

We found station-specific site correction terms for our 6 channels of horizontal and vertical acceleration, velocity, and filtered displacement for stations that contributed more than 3 records to the southern California envelope dataset. Figure 8 shows the station corrections $e_{2ij}$ (in log units) for root mean square horizontal S-wave acceleration amplitudes of selected SCSN stations located on rock sites (Vs30 > 464 m/s) relative to the S-wave acceleration amplitude relationship for rock sites. Also shown are the numbers of records available at the stations, which are indicative of the statistical significance of the corresponding station corrections. Stations PAS, PFO, and ISA have corrections in excess of –0.3 log units, translating to deamplification of greater than 50% relative to the average rock station. Interestingly, all of these stations are advanced seismic observatories; PAS is in a short tunnel cut into granite at the original Seismological Laboratory, ISA is in a goldmine modified for use as a seismic observatory, and PFO is the Pinion Flats observatory operated by UCSD.

The number of records contributing to these corrections (50, 20, and 10 records, respectively) indicates that these corrections are not likely due to randomness or chance, but rather, are evidence of consistent deamplification of root mean square horizontal S-wave accelerations at these sites. Incidentally, this approach allows us to define "average" rock stations whose observed ground motions are closest to those predicted by the best model (or whose station corrections are closest to 0). Some "average" rock stations over the time period 1998-2004 include GSC, PLM, HEC, EDW, and AGA. The set of stations considered "average" by this approach will evolve with time, depending on where seismic activity is concentrated over a given time period. Applying the station corrections on horizontal S-wave amplitudes results in a standard error of regression of $\sigma_{corr}=0.24$, a ~20% reduction relative to the standard error in the uncorrected case, $\sigma_{uncorr}=0.31$.

## Discussion

Using the envelope amplitude attenuation models obtained from the southern California ground motions (Table 1) and the extended magnitude range relationships for PGA and PGV (Table 3), we can compare how different channels of ground motion amplitudes vary as functions of magnitude and distance. We focus the discussion on general characteristics of, and differences between: 1) PGA, PGV, and peak filtered displacement, 2) ground motions on rock versus soil sites, 3) horizontal versus vertical ground motion amplitudes, and 4) P- versus S-wave attenuation.

### *Small amplitude PGA, PGV, and peak filtered displacement*

The S-wavetrain envelope amplitude parameters are comparable to peak amplitudes when examining horizontal ground motion records. The saturation term *C(M)* was designed to come into play at close distances to large events, with regression parameters $c_1$ and $c_2$ controlling the degree of magnitude-dependent saturation effects for M>5. Since *C(M)~0* for M<5 for all components of ground motion, the coefficients *a*, *b*, and *d* can be directly interpreted as the small magnitude (*M<5*) scaling factors for magnitude and distance dependence. Averaging coefficients *a*, *b*, and *d* of rock and soil sites for horizontal acceleration, velocity, and displacement (from Table 1), small amplitude ground motions scale as follows:

$$
\begin{aligned}
&\text{horizontal S-wave acceleration,} && \ddot{u}_S \sim 10^{0.8M} \times 10^{-2.4\times10^{-3} R} \times \frac{1}{R^{1.4}} \\
&\text{horizontal S-wave velocity,} && \dot{u}_S \sim 10^{0.9M} \times 10^{-6.3\times10^{-4} R} \times \frac{1}{R^{1.5}} \\
&\text{horizontal S-wave displacement,} && u_S \sim 10^{1.05M} \times 10^{-6.5\times10^{-7} R} \times \frac{1}{R^{1.5}}
\end{aligned}
\qquad (7)
$$

In general, the geometric spreading term $1/R^d$ is fairly constant for acceleration, velocity and displacement, with *d~1.5*. The effects of the exponential decay term $10^{-yR}$ decrease with frequency; it contributes to the distance decay of peak acceleration, but has practically no effect on the decay of peak displacement amplitudes. This is consistent with high frequency ground motions being more sensitive to small scale crustal heterogeneities and thus exhibiting stronger scattering effects (Lay and Wallace, 1995) , and observations that high frequency ground motions attenuate faster than lower frequency ground motions (Hanks and McGuire, 1981).

*Displacement scaling*

Eqn. (7) indicates that small-amplitude PGA (typically from high frequency ground motions) has a weaker magnitude dependence than small-amplitude PGD (typically from lower frequency ground motions). This is consistent with Brune (1970) spectral scaling, where the high frequency amplitude spectrum scales with $M_o^{1/3}$ and the low frequency spectrum scales with $M_o$ (see Appendix I of Heaton et al (1986) for a discussion of the relationship between peak amplitude and spectral scaling of far-field waves). From simple scaling relations, we expect displacement amplitude *u* to scale with magnitude *M* as $\log u \sim M$ at far field distances (several source dimensions away). This is consistent with magnitude-dependence coefficients, *a*, for horizontal S-wave displacements envelope amplitudes on rock and soil sites being close to 1 (Table 1).

At close distances to large, non-point source events ($M>6$), we expect displacement amplitudes to be proportional to average fault slip (Aagaard et al., 2001) which approximately scales as $M_0^{1/3}$, which implies that $\log u \sim 0.5\, M$. Saturation effects are expected to be significant in this magnitude and distance range. We can define "effective magnitude scaling" (Eqn.8) as the partial derivative of Eqn.(4) with respect to *M*. This effective magnitude scaling is the large amplitude scaling, and takes into account the effects of saturation term, *C(M)*.

$$\frac{\partial \log Y}{\partial M} = a - b\left(\frac{c_1 \exp(c_2(M-5))}{1+(M-5)^2} + C(M)\right) - d\left(\frac{\dfrac{c_1 \exp(c_2(M-5))}{1+(M-5)^2} + C(M)}{R_1 + c_1 \exp(c_2(M-5))\ln(10)}\right) \quad (8)$$

Evaluating Eqn.(8) using the average *a, b,* $c_1$, $c_2$, *d, e* coefficients of rock and soil sites for horizontal S-wave displacement amplitudes, and using $M=6$, $R=0$ *km* to represent the condition "at close distances to large events), yields a value of 0.42. This scaling of $\log u \sim 0.42\, M$ is consistent with the expected scaling of $\log u \sim 0.5\, M$ suggested by simple scaling relations.

Scaling relations from earthquake source physics lead us to anticipate that following asymptotic behavior for any ground motion prediction equations: 1) when distance is large compared to source dimension, low frequency ground motions (displacement *u*) scales with seismic moment:

$$\log u_{far\&lowfreq} \sim \log M_o \sim \frac{3}{2} M \tag{9}$$

2) for near-source, low frequency ground motions, we expect peak displacements to scale with the size of slip, *D*, on nearby fault segments, or

$$\log u_{near\&lowfreq} \sim \log D \sim \log M_o^{1/3} \sim \frac{1}{2} M \tag{10}$$

The displacement scaling from our relationships (subplot c in Figure 9) are consistent with these expectations.

*Rock versus soil sites*

Magnitude-dependence and $1/R^d$ distance attenuation are slightly stronger for ground motions on soil sites for PGA, PGV, and peak filtered displacement (PGD) (Table 1). Saturation effects at close distances to large events are slightly stronger for ground motions recorded on soil sites; the *c1* coefficient for soil is always slightly larger than that for rock ground motions for a given channel. On average, ground motions on soil sites are twice as large as those on rock sites, since the regression coefficient e is consistently ~0.3 log (base10) units larger for soil than rock ground motions. However, ground motion amplification on soil sites relative to rock ground motions is actually both magnitude- and distance-dependent. Figure 9 shows S-wave amplitudes on rock and soil ground motions predicted by our attenuation relationships as functions of magnitude for different distance ranges for acceleration, velocity, and filtered displacement. The PGA and PGV relationships are constrained by the NGA strong motion data; the PGD relationships are based on southern California ground motions only. PGA at close distances to large events exhibit the strongest saturation effects. The total saturation of near-source PGA for large magnitudes is consistent with high frequency ground motions being incoherent noise, independent of magnitude and total slip. This implies that high frequency radiated energy scales with rupture area, which is the Brune (1970) spectral model without the dependence on stress drop. Velocity and displacement ground motions also exhibit saturation, though to a lesser degree than acceleration. The over-saturation of acceleration and velocity amplitudes on soil sites can be attributed to non-linear site effects. This is consistent with the idea that nonlinear soil response contributes to ground motion saturation.

At close distances to large events, the difference in PGA on rock and soil sites decreases with increasing magnitude. This is consistent with the observation of Campbell (1981) that both rock and soil sites subjected to strong shaking tend to record comparable peak accelerations. For PGA, PGV, and PGD, there is no difference between rock and soil ground motions at low amplitude levels (at large distances from small magnitude events).

*P- versus S-waves*

The magnitude and distance dependence of peak P-wave amplitudes, which typically occur on the vertical component, is also represented by Eqn.(4). The small magnitude scaling for P-wave is given by:

$$\begin{aligned}
&\text{vertical P-wave acceleration,} \quad \ddot{u}_P \sim 10^{0.7M} \times 10^{-4.1\times10^{-3}R} \times \frac{1}{R^{1.2}} \\
&\text{vertical P-wave velocity,} \quad \dot{u}_P \sim 10^{0.8M} \times 10^{-4.3\times10^{-4}R} \times \frac{1}{R^{1.4}} \\
&\text{vertical P-wave displacement,} \quad u_P \sim 10^{0.9M} \times 10^{-1.0\times10^{-6}R} \times \frac{1}{R^{1.3}}
\end{aligned} \tag{11}$$

From comparing Eqns.(7) and (11), peak P-wave amplitudes have slightly weaker magnitude dependence, and weaker 1/R decay than peak S-wave amplitudes.

P-wave amplitudes exhibit stronger saturation at close distances to large events than peak S-wave amplitudes (Figure 10). The difference between P- and S-wave amplitudes at close distances to large events increases with as the lower frequency content of the ground motions increase (such that the difference between P- and S-wave amplitudes is largest for PGD). This is consistent with P-waves having more relatively high-frequency energy content, and S-wave having more energy in the lower frequency range. However, it should be noted that the apparent stronger saturation of P-wave amplitudes may also be due to the difficulty in decomposing P- and S-waves at close distances when the time between the S- and P-wave arrivals is small.

*Comparison of extended magnitude range PGA and PGV relationships with other attenuation relationships*

The extended magnitude range attenuation relationships developed in this study are derived from PGA and PGV amplitudes recorded within 200 km of shallow, crustal earthquakes in active tectonic regions in the magnitude range $2 \leq M < 8$. These relationships are among the first ground motion prediction equations that are valid over such a wide magnitude range. (Bommer et al (2007) develop prediction equations for response spectral accelerations at various periods covering the magnitude range $3 \leq M \leq 7.6$ using a European and Middle Eastern dataset.)

We compare the median ground motion levels predicted by our extended magnitude range relationships with those predicted by the Boore and Atkinson (2008) and Campbell and Bozorgnia (2008) NGA relationships, and the ShakeMap small amplitude relationship (Wald et al., 1999; 2005) . We will refer to these relationships as BA2008, CB2008, and SM2005, respectively.

To evaluate the BA2008 equations, we use the "unknown" faulting coefficients for PGA and PGV. To evaluate the CB2008 equations, we assume a vertical strike slip fault ($dip=90°$, $rake=0°$) and the following values recommended by the developers: $Z_{tor}=5$ *km for* $M=5$, $Z_{tor}=0$ *km for* $M=7$, $Z_{2.5}=2.0$. We refer the reader to Campbell and Bozorgnia (2008) for explanations of their various predictor variables. Both BA2008 and CB2008 use the average shear wave velocity in the upper 30 meters (Vs30) as a predictor variable. When comparing the median ground motions from the NGA relationships with those from our rock relationships, we evaluate BA2008 and CB2008 with Vs30=554 m/s, which is the median Vs30 value for sites with Vs30 > 464 m/s in the NGA database. We use Vs30=308 m/s to evaluate the NGA relationships when comparing with our soil relationships.

Figure 11 shows the predicted PGA and PGV levels from the extended magnitude range relationships from this study, BA2008, and CB2008 at $M = 6.75$ for rock (Vs30 > 464m/s) and soil sites (Vs30 < 464m/s), as well as the observed values in the magnitude range $6.5 \leq M \leq 7.0$ from the NGA database and the southern California envelope dataset. The median PGA predicted for $M=6.75$ are fairly consistent between the 3 relationships, and are consistent with the observed PGA and PGV in the $6.5 \leq M \leq 7.0$ magnitude range, which are primarily from the NGA database. The apparent consistency between BA2008, CB2008, and our relationships for large magnitude earthquakes is expected, since each of these studies were intended to fit approximately the same data at large magnitudes.

Figure 12 shows that when considering the magnitude range $2 \leq M < 8$, there are significant differences between our relationships and any of other relationships that were intended to predict motions in a restricted magnitude band. The discrepancies between our extended magnitude relationships and the NGA relationships (BA2008 and CB2008) at the $M=5$ level may be attributed to the different datasets used to constrain the respective regressions. *M=5* is the lower bound of the magnitude range in which the BA2008 and CB2008 relationships are recommended to be used by their developers. Most of the data used to constrain the NGA relationships are from *M>5* events, thus observations available to constrain median *M=5* ground motion levels in the NGA relationships are primarily from *M>5* events. In contrast, the median *M=5* ground motions from the our extended magnitude range relationships are constrained by significantly more data (from the southern California envelope dataset) in the *4.5 < M < 5.5 range.*

*Conversion factors between selected definitions of horizontal ground motion*

Several definitions of horizontal ground motion have been mentioned thus far. The NGA relationships use "GMIrot50", a flavor of geometric mean independent of station orientation proposed by Boore et al (2006). Beyer and Bommer (2006) found that "GMIrot50" is virtually identical to the geometric mean of the peak ground motions from 2 horizontal, orthogonally oriented instruments (gm); $gm \equiv \sqrt{\max_{time}\left(U_N\right)\max_{time}\left(U_E\right)}$. In the envelope analysis conducted in this study, we used the root mean square of horizontal envelope amplitudes (rms) to combine information from 2 horizontal channels (typically North-South and East-West orientations) into a single horizontal ground motion measure. In our definition of rms amplitude, we combine the peak values of two horizontal components; $rms \equiv \sqrt{\frac{1}{2}\left\{\left[\max_{time}\left(U_N\right)\right]^2 + \left[\max_{time}\left(U_E\right)\right]^2\right\}}$. Since these peak values are defined over time (for efficient data transfer for early warning applications), our definition of rms is approximately $\sqrt{1/2}$ times larger than the peak of the vector amplitude (va), which is a scalar invariant that is probably the best way to measure amplitude; $va \equiv \max_{time} \sqrt{U_N^2 + U_E^2}$. The ShakeMap codes use the larger of the 2 maximum amplitude values over time available from 2 horizontal channels (*maxEnv* – borrowing terminology from Beyer and Bommer (2006)), $\max ENV \equiv \max_{time}\left(U_N, U_E\right)$. While most strong motion attenuation relationships predict horizontal ground motions in terms of geometric mean (gm), or random horizontal component (random), the maximum ground motions experienced by structures during an earthquake are due to the vector amplitude (va) of the horizontal ground motions, which is larger than any of the other definitions thus far mentioned. We used the waveforms in our southern California database ($2 < M \leq 7.3$) to calculate the maximum vector amplitude of broadband acceleration and velocity over time, and compare this measure with some commonly-used horizontal measures: the maximum of a random horizontal component (*rand*), the root mean square (*rms*), the geometric mean (*gm*), and the larger (*maxEnv* – borrowing terminology from Beyer and Bommer (2006)) of the maximums over time on 2 horizontal channels. Equations for these various definitions of horizontal ground motion are listed in Table 4. Recent papers on conversion factors between different definitions of horizontal ground motions include Beyer and Bommer (2006) and Watson-Lamprey, and Boore (2007). This work differs from those studies in the datasets used, magnitude ranges considered, and application emphasis. Our conversion factors are obtained from southern California waveforms from events in the magnitude range $2 < M \leq 7.3$, with a considerable larger number of $M<5$ events. We focus primarily on PGA and PGV due to our interests in earthquake early warning and real-time applications. Note that what we call the maximum vector amplitude is called MaxD by Beyer and Bommer (2006) and SaMaxRot by Watson-Lamprey and Boore (2007).

Tables 5.1 and 5.2 list the conversion factors derived in this study between various horizontal component definitions for PGA and PGV. The median ratios listed are multiplicative factors that can be used to convert from a median component definition in the column headings to a median component definition on a given row. For instance, for PGA (first row, Table 5.1), the vector amplitude is 1.17 times larger than the geometric mean. The $\sigma$ values listed are the standard deviation of the $\log_{10}$ ratios. The conversion factors and $\sigma$ values from geometric mean to other definitions from Beyer and Bommer (2006) and Watson-Lamprey and Boore (2007) are also listed. In general, the conversion factors common to the three studies are consistent, suggesting that these ratios are relatively independent of magnitude. The ratios between vector amplitude and geometric and root mean square definitions can be described by a Gaussian distribution, while ratios between vector amplitude and random horizontal component and maxEnv are better described by a Gamma distribution (Figure 13). The distribution of the ratios is similar for both PGA and PGV.

Beyer and Bommer (2006) use the following relationship to modify the uncertainty parameter $\sigma$ in an attenuation relationship when converting from horizontal component definition b to a:

$$\sigma^2_{tot,\log Y_a} = \sigma^2_{\log Y_b}\left(\frac{\sigma_{\log Y_a}}{\sigma_{\log Y_b}}\right)^2 + \sigma^2_{\log Y_a/Y_b} \tag{12}$$

$\sigma \log Y_b$ is the uncertainty or variability from the horizontal component definition one is starting from. $\sigma \log Y_a/Y_b$ are the values tabulated in Tables 5.1 and 5.2. One can perform regression analyses on a given dataset using various horizontal component definitions to find the ($\sigma \log Y_a/\sigma \log Y_b$) term. We did not solve for these ratios in this study, and recommend using the ($\sigma \log Y_a/\sigma \log Y_b$) values of Beyer and Bommer when applicable, and $\sigma \log Y_a/\sigma \log Y_b=1$ otherwise. Beyer and Bommer (2006) find that these ratios are not large, and would be significant if low probabilities of exceedence were being considered. However, since the primary application we are concerned with is earthquake early warning and other real-time applications, we believe the simplification of $\sigma \log Y_a/\sigma \log Y_b=1$ when necessary is justified.

**Conclusions**

We applied an envelope-based parameterization of ground motion envelopes to waveform data from 70 southern California earthquakes, and developed predictive relationships for the shape of ground motion envelope amplitudes as a function of time for 6 channels of ground motion - horizontal and vertical acceleration, velocity, and filtered displacement. Of the 11 envelope parameters utilized, the P- and S-wave envelope amplitudes, which characterize peak P- and S-wave amplitude levels, displayed the most significant magnitude and distance dependence. We developed attenuation relationships for P- and S-wave amplitudes as functions of magnitude, distance, and site for 6 channels of ground motion, and used these relationships to explore general characteristics of southern California ground motions. We developed relationships that capture peak amplitude scaling of P- and S-wave acceleration, velocity, and filtered displacement over the magnitude range $2 \leq M \leq 7.3$. We found that S-wave acceleration amplitudes (equivalent to PGA) on soil sites tends to approach the S-wave acceleration amplitudes on rock sites at close distances to large events, providing evidence of nonlinear site amplification. Mid- to longer period ground motions (S-wave velocity and filtered displacement amplitudes) also exhibit a change in scaling at close distances to large events.

We combined our horizontal S-wave acceleration and velocity envelope amplitude dataset with the NGA strong motion dataset to develop relationships for PGA and PGV that span the magnitude range $2 \leq M < 8$. The median PGA and PGV values predicted by our extended magnitude range relationships are comparable to those from the NGA relationships (Boore and Atkinson, 2008; Campbell and Bozorgnia 2008) at the larger magnitudes, and with the ShakeMap (Wald et al., 1999; Wald et al., 2005) small amplitude relationships at the lower magnitude range. We find that the BA2006 and CB2007 relationships systematically over-predict ground motions at the $M=5$ level, which is the lower end of the magnitude range of recommended use by their developers. This is consistent with Bommer et al (2007), who suggest that the data used to constrain attenuation relationships should be at least 1 magnitude unit lower than the lower limit of magnitude for which the relationships would be used. The extended magnitude range relationships for PGA and PGV derived in this study can be used in earthquake early warning and ShakeMap-type applications that need to operate on the more frequent small earthquakes as well as the infrequent but more damaging events. Using an extended magnitude range allows our ground motion prediction equations to capture scaling characteristics that are consistent with earthquake source physics. These characteristics are not evident when considering data in more limited magnitude ranges.

We also derived conversion factors between various definitions of horizontal peak ground motion using our southern California waveform dataset ($2 \leq M \leq 7.3$), similar to recent studies by Beyer and Bommer (2006) and Watson-Lamprey and Boore (2007) on subsets of the NGA database. Conversion factors from these 3 studies are quite consistent with each other, suggesting that these conversion factors are not strongly dependent on magnitude.

**Acknowledgements**

We wish to thank David Boore and Kenneth Campbell for providing and answering questions about their NGA models, Julian Bommer for providing preprints of his manuscripts, David Wald for interesting and informative discussions on attenuation relationships and help with the ShakeMap codes, and Egill Hauksson for the extensive use of his computers for running the neighborhood algorithm inversions. We also wish to thank John Clinton for his suggestions on improving early versions of the manuscript.

This work was supported at various stages by the George W. Housner Fellowship at the California Institute of Technology, the Puerto Rico Strong Motion Program, and the Swiss Seismological Service at the Swiss Federal Institute of Technology (ETH Zurich).

**References**


Aagaard, B. T., Hall, J. F., & Heaton, T. H. (2001). Characterization of Near-Source Ground Motions with Earthquake Simulations. *Earthquake Spectra, 17*(2), 177-207.

Beyer, K., & Bommer, J. J. (2006). Relationships between Median Values and between Aleatory Variabilities for Different Definitions of the Horizontal Component of Motion. *Bulletin of the Seismological Society of America, 96*(4A), 1512-1522.

Bommer, J. J., Stafford, P. J., Alarcon, J. E., & Akkar, S. (2007). The Influence of Magnitude Range on Empirical Ground-Motion Prediction. *Bulletin of the Seismological Society of America, 97*(6), 2152-2170.

Boore, D., & Atkinson, G. (2008). Ground-motion prediction equations for the average horizontal component of PGA, PGV, and 5%-damped PSA at spectral periods between 0.01s and 10.0 s. *Earthquake Spectra, NGA Special Volume*.

Boore, D., Joyner, W. B., & Fumal, T. E. (1997). Equations for estimating horizontal response spectra and peak acceleration from western North American earthquakes: a summary of recent work. *Seismological Research Letters, 68*, 128-153.

Boore, D., Watson-Lamprey, J., & Abrahamson, N. (2006). Orientation-Independent Measures of Ground Motion. *Bulletin of the Seismological Society of America, 96*(4A), 1502-1511.

Boore, D. M., & Joyner, W. B. (1982). The empirical prediction of ground motion. *Bulletin of the Seismological Society of America, 72*(6B), S43-60.

Brune, J. N. (1970). Tectonic stress and the spectra of seismic shear waves from earthquakes. *Journal of Geophysical Research, 75*, 4997-5009.

Campbell, K., & Bozorgnia, Y. (2008). NGA ground motion model for the geometric mean horizontal component of PGA, PGV, PGD, and 5% damped linear elastic response spectra for periods ranging from 0.01 to 10s. *Earthquake Spectra, NGA Special Volume*.

Campbell, K. W. (1981). Near-source attenuation of peak horizontal acceleration. *Bulletin of the Seismological Society of America, 71*(6), 2039-2070.

Campbell, K. W. (2004). Prediction of Strong Ground Motion Using the Hybrid Empirical Method and Its Use in the Development of Ground-Motion (Attenuation) Relations in Eastern North America. *Bulletin of the Seismological Society of America, 94*(6), 2418.

Cua, G. B. (2005). *Creating the Virtual Seismologist : developments in ground motion characterization and seismic early warning.* California Institute of Technology, Pasadena, Calif.

Hadley, D. M., & Helmberger, D. V. (1980). Simulation of strong ground motions. *Bulletin of the Seismological Society of America, 70*(2), 617-630.

Hanks, T. C., & McGuire, R. K. (1981). The character of high-frequency strong ground motion. *Bulletin of the Seismological Society of America, 71*(6), 2071-2095.

Heaton, T. H., Tajima, F., & Wildenstein Mori, A. (1986). Estimating ground motions using recorded accelerograms. *Surveys in Geophysics, 8*(1), 25-83.

http://db.cosmos-eq.org. Consortium of Organizations for Strong-Motion Observation Systems (Publication.: http://db.cosmos-eq.org http://peer.berkeley.edu/nga. NGA Database. from http://peer.berkeley.edu/nga/

http://www.data.scec.org. Southern California Earthquake Data Center. from http://www.data.scec.org

Jennings, P., Housner, G., & Tsai, N. (1968). *Simulated earthquake motions.* Pasadena: California Institute of Technology.

Lay, T., & Wallace, T. (1995). *Modern Global Seismology*: Academic Press.

Mori, J., Kanamori, H., Davis, J., Hauksson, E., Clayton, R., Heaton, T., et al. (1998). Major improvements in progress for southern California earthquake monitoring. *Eos, Transactions American Geophysical Union, 79*(18), 217.

Power, M., Chiou, B., Abrahamson, N., Bozorgnia, Y., Shantz, T., & Roblee, C. (2008). An overview of the NGA project. *Earthquake Spectra, NGA Special Volume*.

Richter, C. F. (1935). An instrumental earthquake magnitude scale. *Bulletin of the Seismological Society of America, 25*(1), 1-32.

Sambridge, M. (1999a). Geophysical Inversion with a Neighborhood Algorithm - I. Searching a parameter space. *Geophysics Journal Interational, 138*, 479-494.

Sambridge, M. (1999b). Geophysical Inversion with a Neighborhood Algorithm -II. Appraising the ensemble. *Geophysics Journal International, 138*, 727-746.

Wald, D. J., Quitoriano, V., Heaton, T., Kanamori, H., Scrivner, C. W., & Worden, B. C. (1999). TriNet "ShakeMaps": rapid generation of peak ground motion and intensity maps for earthquakes in southern California. *Earthquake Spectra, 15*(3), 537-556.

Wald, D. J., Worden, B. C., Quitoriano, V., & Pankow, K. (2005). *ShakeMap Manual: Technical Manual, User's Guide, and Software Guide*: US Geological Survey.

Wills, C. J., Petersen, M., Bryant, W. A., Reichle, M., Saucedo, G. J., Tan, S., et al. (2000). A Site-Conditions Map for California Based on Geology and Shear-Wave Velocity. *Bulletin of the Seismological Society of America, 90*(6B), S187-208.

Yamada, M., Heaton, T., & Beck, J. (2007). Real-Time Estimation of Fault Rupture Extent Using Near-Source versus Far-Source Classification. *Bulletin of the Seismological Society of America, 97*(6), 1890-1910.

**Tables**

Table 1

Attenuation relationships for ground motion envelope amplitudes

$$\log Y = aM + b(R_1 + C(M)) + d\log\ (R_1 + C(M)) + e$$

$$R_1 = \sqrt{R^2 + 9}$$

$$C(M) = c_1 \exp(c_2(M - 5)) \times (\arctan(M - 5) + \tfrac{\pi}{2})$$

| | | | | a | b | $c_1$ | $c_2$ | d | e | σ |
|---|---|---|---|---|---|---|---|---|---|---|
| Root mean square horizontal amplitudes | P-wave | Acceleration | rock | 0.72 | $-3.3\text{x}10^{-3}$ | 1.6 | 1.05 | -1.2 | -1.06 | 0.31 |
| | | | soil | 0.74 | $-2.5\text{x}10^{-3}$ | 2.41 | 0.95 | -1.26 | -1.05 | 0.29 |
| | | velocity | rock | 0.80 | $-8.4\text{x}10^{-4}$ | 0.76 | 1.03 | -1.24 | -3.103 | 0.27 |
| | | | soil | 0.84 | $-5.4\text{x}10^{-4}$ | 1.21 | 0.97 | -1.28 | -3.13 | 0.26 |
| | | displacement | rock | 0.95 | $-1.7\text{x}10^{-7}$ | 2.16 | 1.08 | -1.27 | -4.96 | 0.28 |
| | | | soil | 0.94 | $-5.17\text{x}10^{-7}$ | 2.26 | 1.02 | -1.16 | -5.01 | 0.3 |
| | S-wave | acceleration | rock | 0.78 | $-2.6\text{x}10^{-3}$ | 1.48 | 1.11 | -1.35 | -0.64 | 0.31 |
| | | | soil | 0.84 | $-2.3\text{x}10^{-3}$ | 2.42 | 1.05 | -1.56 | -0.34 | 0.31 |
| | | velocity | rock | 0.89 | $-4.3\text{x}10^{-4}$ | 1.11 | 1.11 | -1.44 | -2.60 | 0.28 |
| | | | soil | 0.96 | $-8.3\text{x}10^{-4}$ | 1.98 | 1.06 | -1.59 | -2.35 | 0.30 |
| | | displacement | rock | 1.03 | $-1.01\text{x}10^{-7}$ | 1.09 | 1.13 | -1.43 | -4.34 | 0.27 |
| | | | soil | 1.08 | $-1.2\text{x}10^{-6}$ | 1.95 | 1.09 | -1.56 | -4.1 | 0.32 |
| Vertical amplitudes | P-wave | acceleration | rock | 0.74 | $-4.01\text{x}10^{-3}$ | 1.75 | 1.09 | -1.2 | -0.96 | 0.29 |
| | | | soil | 0.74 | $-5.17\text{x}10^{-7}$ | 2.03 | 0.97 | -1.2 | -0.77 | 0.31 |
| | | velocity | rock | 0.82 | $-8.54\text{x}10^{-4}$ | 1.14 | 1.10 | -1.36 | -2.901 | 0.26 |
| | | | soil | 0.81 | $-2.65\text{x}10^{-6}$ | 1.4 | 1.0 | -1.48 | -2.55 | 0.30 |
| | | displacement | rock | 0.96 | $-1.98\text{x}10^{-6}$ | 1.66 | 1.16 | -1.34 | -4.79 | 0.28 |
| | | | soil | 0.93 | $-1.09\text{x}10^{-7}$ | 1.5 | 1.04 | -1.23 | -4.74 | 0.31 |
| | S-wave | acceleration | rock | 0.78 | $-2.7\text{x}10^{-3}$ | 1.76 | 1.11 | -1.38 | -0.75 | 0.30 |
| | | | soil | 0.75 | $-2.47\text{x}10^{-3}$ | 1.59 | 1.01 | -1.47 | -0.36 | 0.30 |
| | | velocity | rock | 0.90 | $-1.03\text{x}10^{-3}$ | 1.39 | 1.09 | -1.51 | -2.78 | 0.25 |
| | | | soil | 0.88 | $-5.41\text{x}10^{-4}$ | 1.53 | 1.04 | -1.48 | -2.54 | 0.27 |
| | | displacement | rock | 1.04 | $-1.12\text{x}10^{-5}$ | 1.38 | 1.18 | -1.37 | -4.74 | 0.25 |
| | | | soil | 1.03 | $-4.92\text{x}10^{-6}$ | 1.55 | 1.08 | -1.36 | -4.57 | 0.28 |

Table 2.1
Horizontal P-wave envelope attenuation relationship for rise time, duration, decay parameters

$$\log(env\_param) = \alpha M + \beta R + \delta \log R + \mu$$
$$env\_param = \{tr, \Delta t, \tau, \gamma\}$$

| | | | α | β | δ | μ | σ |
|---|---|---|---|---|---|---|---|
| acceleration | rock | *tr* | 0.06 | 5.50x10-4 | 0.27 | -0.37 | 0.22 |
| | | $\Delta t$ | - | 2.58x10-3 | 0.21 | -0.22 | 0.39 |
| | | $\tau$ | 0.047 | - | 0.48 | -0.75 | 0.28 |
| | | $\gamma$ | -0.032 | -1.81x10-3 | -0.1 | 0.64 | 0.16 |
| | soil | *tr* | 0.07 | 1.2x10-3 | 0.24 | -0.38 | 0.26 |
| | | $\Delta t$ | 0.03 | 2.37x10-3 | 0.39 | -0.59 | 0.36 |
| | | $\tau$ | 0.087 | -1.89x10-3 | 0.58 | -0.87 | 0.31 |
| | | $\gamma$ | -0.48 | -1.42x10-3 | -0.13 | 0.71 | 0.21 |
| velocity | rock | *tr* | 0.06 | 1.33x10-3 | 0.23 | -0.34 | 0.25 |
| | | $\Delta t$ | 0.054 | 1.93x10-3 | 0.16 | -0.36 | 0.40 |
| | | $\tau$ | 1.86x10-2 | 5.37x10-5 | 0.41 | -0.51 | 0.30 |
| | | $\gamma$ | -0.044 | -1.65x10-3 | -0.16 | 0.72 | 0.20 |
| | soil | *tr* | 0.07 | 4.35x10-4 | 0.47 | -0.68 | 0.26 |
| | | $\Delta t$ | 0.03 | 2.03x10-3 | 0.289 | -0.45 | 0.40 |
| | | $\tau$ | 0.0403 | -1.26x10-3 | 0.387 | -0.372 | 0.37 |
| | | $\gamma$ | -6.17x10-2 | -2.0x10-3 | - | 0.578 | 0.25 |
| displacement | rock | *tr* | 0.05 | 1.29x10-3 | 0.27 | -0.34 | 0.28 |
| | | $\Delta t$ | 0.047 | - | 0.45 | -0.68 | 0.43 |
| | | $\tau$ | - | - | 0.19 | -0.07 | 0.39 |
| | | $\gamma$ | -0.062 | -2.3x10-3 | - | 0.61 | 0.26 |
| | soil | *tr* | 0.05 | 1.19x10-3 | 0.47 | -0.58 | 0.26 |
| | | $\Delta t$ | 0.051 | 1.12x10-3 | 0.33 | -0.59 | 0.41 |
| | | $\tau$ | 0.035 | -1.27x10-3 | 0.19 | 0.03 | 0.43 |
| | | $\gamma$ | -0.061 | -1.9x10-3 | 0.11 | 0.39 | 0.31 |

Table 2.2
Horizontal S-wave envelope attenuation relationship for rise time, duration, decay parameters

$$\log(env\_param) = \alpha M + \beta R + \delta \log R + \mu$$
$$env\_param = \{tr, \Delta t, \tau, \gamma\}$$

| | | | α | β | δ | μ | σ |
|---|---|---|---|---|---|---|---|
| acceleration | rock | *tr* | 0.64 | - | 0.48 | -0.89 | 0.23 |
| | | *Δt* | - | -4.87x10-4 | 0.13 | 0.0024 | 0.2 |
| | | $\tau$ | 0.037 | - | 0.39 | -0.59 | 0.18 |
| | | $\gamma$ | -0.014 | -5.28x10-4 | -0.11 | 0.26 | 0.09 |
| | soil | *tr* | 0.055 | 1.21x10-3 | 0.34 | -0.66 | 0.25 |
| | | *Δt* | 0.028 | - | 0.07 | -0.102 | 0.23 |
| | | $\tau$ | 0.0557 | -8.2x10-4 | 0.51 | -0.68 | 0.24 |
| | | $\gamma$ | -0.015 | -5.89x10-4 | -0.163 | 0.23 | 0.13 |
| velocity | rock | *tr* | 0.093 | - | 0.48 | -0.96 | 0.25 |
| | | *Δt* | 0.02 | - | - | 0.046 | 0.23 |
| | | $\tau$ | 0.029 | 8.0x10-4 | 0.25 | -0.31 | 0.23 |
| | | $\gamma$ | -0.024 | -1.02x10-3 | -0.06 | 0.21 | 0.11 |
| | soil | *tr* | 0.087 | 4.0x10-4 | 0.49 | -0.98 | 0.30 |
| | | *Δt* | 0.028 | - | 0.05 | -0.08 | 0.23 |
| | | $\tau$ | 0.045 | -5.46x10-4 | 0.46 | -0.55 | 0.25 |
| | | $\gamma$ | -0.031 | -4.61x10-4 | -0.162 | 0.30 | 0.13 |
| displacement | rock | *tr* | 0.109 | 7.68x10-4 | 0.38 | -0.87 | 0.29 |
| | | *Δt* | 0.04 | 1.1x10-3 | -0.15 | 0.11 | 0.23 |
| | | $\tau$ | 0.029 | - | 0.36 | -0.38 | 0.26 |
| | | $\gamma$ | -0.025 | -4.22x10-4 | -0.145 | 0.262 | 0.12 |
| | soil | *tr* | 0.12 | - | 0.45 | -0.89 | 0.34 |
| | | *Δt* | 0.03 | - | 0.037 | -0.066 | 0.28 |
| | | $\tau$ | 0.038 | -1.34x10-3 | 0.48 | -0.39 | 0.30 |
| | | $\gamma$ | -2.67x10-2 | 2.0x10-4 | -0.22 | 0.27 | 0.14 |

Table 2.3
Vertical P-wave envelope attenuation relationship
for rise time, duration, decay parameters

$$\log(env\_param) = \alpha M + \beta R + \delta \log R + \mu$$

$$env\_param = \{tr, \Delta t, \tau, \gamma\}$$

| | | | α | β | δ | μ | σ |
|---|---|---|---|---|---|---|---|
| acceleration | rock | *tr* | 0.06 | 7.45x10-4 | 0.37 | -0.51 | 0.22 |
| | | *Δt* | - | 2.75x10-3 | 0.17 | -0.24 | 0.41 |
| | | $\tau$ | 0.03 | - | 0.58 | -0.97 | 0.26 |
| | | $\gamma$ | -0.027 | -1.75x10-3 | -0.18 | 0.74 | 0.15 |
| | soil | *tr* | 0.06 | 5.87x10-4 | 0.23 | -0.37 | 0.23 |
| | | *Δt* | - | 1.76x10-3 | 0.36 | -0.48 | 0.41 |
| | | $\tau$ | 0.057 | -1.36x10-3 | 0.63 | -0.96 | 0.28 |
| | | $\gamma$ | -0.024 | -1.6x10-3 | -0.24 | 0.84 | 0.18 |
| velocity | rock | *tr* | 0.06 | 7.32x10-4 | 0.25 | -0.37 | 0.26 |
| | | *Δt* | 0.046 | 2.61x10-3 | - | -0.21 | 0.41 |
| | | $\tau$ | 0.03 | 8.6x10-4 | 0.35 | -0.62 | 0.29 |
| | | $\gamma$ | -0.039 | -1.9x10-3 | -0.18 | 0.76 | 0.18 |
| | soil | *tr* | 0.06 | 1.1x10-3 | 0.22 | -0.36 | 0.24 |
| | | *Δt* | 0.031 | 1.7x10-3 | 0.26 | -0.52 | 0.42 |
| | | $\tau$ | 0.31 | -6.4x10-4 | 0.44 | -0.55 | 0.32 |
| | | $\gamma$ | -0.037 | -2.23x10-3 | -0.14 | 0.71 | 0.22 |
| displacement | rock | *tr* | 0.08 | 1.63x10-3 | 0.13 | -0.33 | 0.27 |
| | | *Δt* | 0.058 | 2.02x10-3 | - | -0.25 | 0.42 |
| | | $\tau$ | 0.05 | 8.9x10-4 | 0.16 | -0.39 | 0.36 |
| | | $\gamma$ | -0.052 | -1.67x10-3 | -0.21 | 0.85 | 0.22 |
| | soil | *tr* | 0.067 | 1.21x10-3 | 0.28 | -0.46 | 0.27 |
| | | *Δt* | 0.043 | 9.94x10-4 | 0.19 | -0.42 | 0.41 |
| | | $\tau$ | 0.052 | - | 0.12 | -0.17 | 0.39 |
| | | $\gamma$ | -0.7 | -2.5x10-3 | - | 0.63 | 0.27 |

Table 2.4
Vertical S-wave envelope attenuation relationship for rise time, duration, decay parameters

$$\log(env\_param) = \alpha M + \beta R + \delta \log R + \mu$$
$$env\_param = \{tr, \Delta t, \tau, \gamma\}$$

| | | | α | β | δ | μ | σ |
|---|---|---|---|---|---|---|---|
| acceleration | rock | *tr* | 0.069 | - | 0.49 | -0.97 | 0.23 |
| | | *Δt* | 0.03 | -1.4x10-3 | 0.22 | -0.17 | 0.20 |
| | | *τ* | 0.031 | - | 0.34 | -0.44 | 0.19 |
| | | *γ* | 0.015 | -4.64x10-4 | -0.12 | 0.26 | 0.095 |
| | soil | *tr* | 0.059 | 2.18x10-3 | 0.26 | -0.66 | 0.25 |
| | | *Δt* | 0.03 | -1.78x10-3 | 0.31 | -0.31 | 0.25 |
| | | *τ* | 0.06 | -1.45x10-3 | 0.51 | -0.6 | 0.22 |
| | | *γ* | -0.02 | - | -0.24 | 0.38 | 0.13 |
| velocity | rock | *tr* | 0.12 | - | 0.50 | -1.14 | 0.27 |
| | | *Δt* | 0.018 | - | - | -0.072 | 0.23 |
| | | *τ* | 0.04 | 9.4x10-4 | 0.25 | -0.34 | 0.23 |
| | | *γ* | -0.028 | -8.32x10-4 | -0.12 | 0.32 | 0.11 |
| | soil | *tr* | 0.11 | 1.24x10-3 | 0.38 | -0.91 | 0.31 |
| | | *Δt* | 0.017 | -6.93x10-4 | 0.12 | -0.05 | 0.27 |
| | | *τ* | 0.051 | -1.41x10-3 | 0.44 | -0.37 | 0.26 |
| | | *γ* | -0.03 | - | -0.21 | 0.33 | 0.15 |
| displacement | rock | *tr* | 0.12 | 1.3x10-3 | 0.26 | -0.75 | 0.30 |
| | | *Δt* | 0.03 | 2.6x10-4 | - | -0.02 | 0.25 |
| | | *τ* | 0.02 | - | 0.30 | -0.22 | 0.26 |
| | | *γ* | -0.02 | - | -0.23 | 0.31 | 0.12 |
| | soil | *tr* | 0.12 | - | 0.44 | -0.82 | 0.40 |
| | | *Δt* | 0.02 | -7.18x10-4 | 0.07 | -0.005 | 0.26 |
| | | *τ* | 0.022 | -1.65x10-3 | 0.44 | -0.19 | 0.28 |
| | | *γ* | -0.018 | 5.65x10-4 | -0.25 | 0.24 | 0.14 |

Table 3
Extended magnitude range attenuation relationships

$$\log Y = aM + b(R_1 + C(M)) + d\log(R_1 + C(M)) + e$$
$$R_1 = \sqrt{R^2 + 9}$$
$$C(M) = c_1 \exp(c_2(M-5)) \times (\arctan(M-5) + \tfrac{\pi}{2})$$

| | | a | b | $c_1$ | $c_2$ | d | e | σ |
|---|---|---|---|---|---|---|---|---|
| PGA | rock | 0.73 | -7.2x10-4 | 1.16 | 0.96 | -1.48 | -0.42 | 0.31 |
| | soil | 0.71 | -2.38x10-3 | 1.72 | 0.96 | -1.44 | -2.45x10-2 | 0.33 |
| PGV | rock | 0.86 | -5.58x10-4 | 0.84 | 0.98 | -1.37 | -2.58 | 0.28 |
| | soil | 0.89 | -8.4x10-4 | 1.39 | 0.95 | -1.47 | -2.24 | 0.32 |

Table 4
Various definitions of maximum horizontal ground motion mentioned in this study

$U_N$ and $U_E$ denote ground motion time series recorded by two orthgonally-oriented horizontal instruments (typically in the North-South and East-West directions).

| Name | Definition |
|---|---|
| Vector amplitude (va) | $\max_{time}\sqrt{U_N^2 + U_E^2}$ |
| Geometric mean (gm) | $\sqrt{\max_{time}(U_N) \times \max_{time}(U_E)}$ |
| Larger of 2 horizontal Components (maxEnv) | $\max(\max_{time}(U_N), \max_{time}(U_E))$ |
| Random horizontal component (rand) | $random(\max_{time}(U_N), \max_{time}(U_E))$ |
| Root mean square (rms) | $\sqrt{\frac{1}{2}\left\{\left[\max_{time}(U_N)\right]^2 + \left[\max_{time}(U_E)\right]^2\right.}$ |
| GMIRot50 | See Boore et al (2006) |

Table 5.1

Median conversion factors and standard deviation of log ratios for PGA between selected definitions of horizontal ground motion components. First entries in each cell are from this study.

| | maxEnv median | maxEnv σ | rand median | rand σ | rms median | rms σ | gm median | gm σ |
|---|---|---|---|---|---|---|---|---|
| Vector (va) | 1.04 | 0.03 | 1.15 | 0.07 | 1.17 | 0.03 | 1.18<br>[1.20<br>[1.20 | 0.04<br>0.04]†<br>0.04]§ |
| maxEnv | | | 1.00 | 0.08 | 1.09 | 0.03 | 1.10<br>[1.10 | 0.04<br>0.05]† |
| rand | | | | | 1.00 | 0.07 | 1.00<br>[1.00 | 0.06<br>0.07]† |
| rms | | | | | | | 1.01 | 0.01 |

† from Beyer and Bommer (2006), § fromWatson-Lamprey and Boore (2007)

Table 5.2

Median conversion factors and standard deviation of log ratios for PGV between selected definitions of horizontal ground motion components. First entries in each cell are from this study.

| | maxEnv median | maxEnv σ | rand median | rand σ | rms median | rms σ | gm median | gm σ |
|---|---|---|---|---|---|---|---|---|
| Vector (va) | 1.04 | 0.03 | 1.15 | 0.08 | 1.18 | 0.03 | 1.20<br>[1.25 | 0.04<br>0.05]† |
| maxEnv | | | 1.00 | 0.08 | 1.10 | 0.03 | 1.11<br>[1.15 | 0.04<br>0.06]† |
| rand | | | | | 1.00 | 0.07 | 1.00<br>[1.00 | 0.07<br>0.09]† |
| rms | | | | | | | 1.01 | 0.01 |

† from Beyer and Bommer (2006)

## Figures

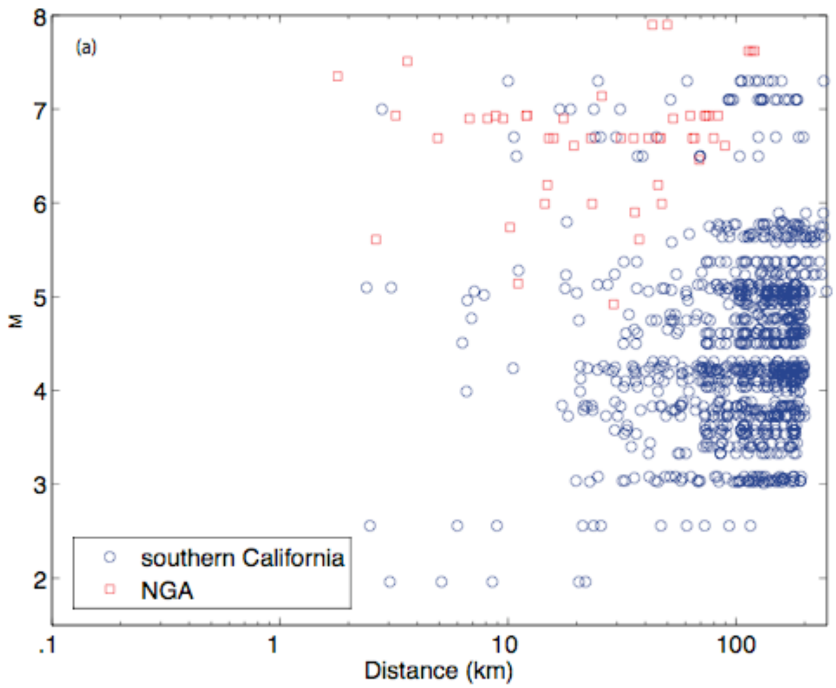


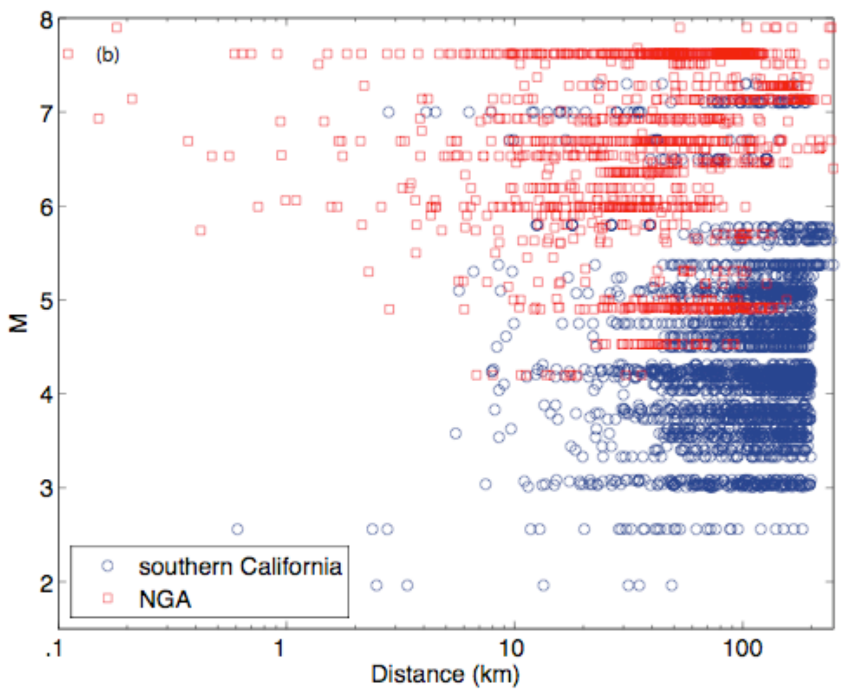


Figure 1: Distribution in magnitude and distance space of NGA strong motion dataset and southern California envelope dataset on sites with a) Vs30 > 464 m/s (NEHRP site classes BC and above), and b) Vs30 ≤ 464 m/s (NEHRP site class C and below)

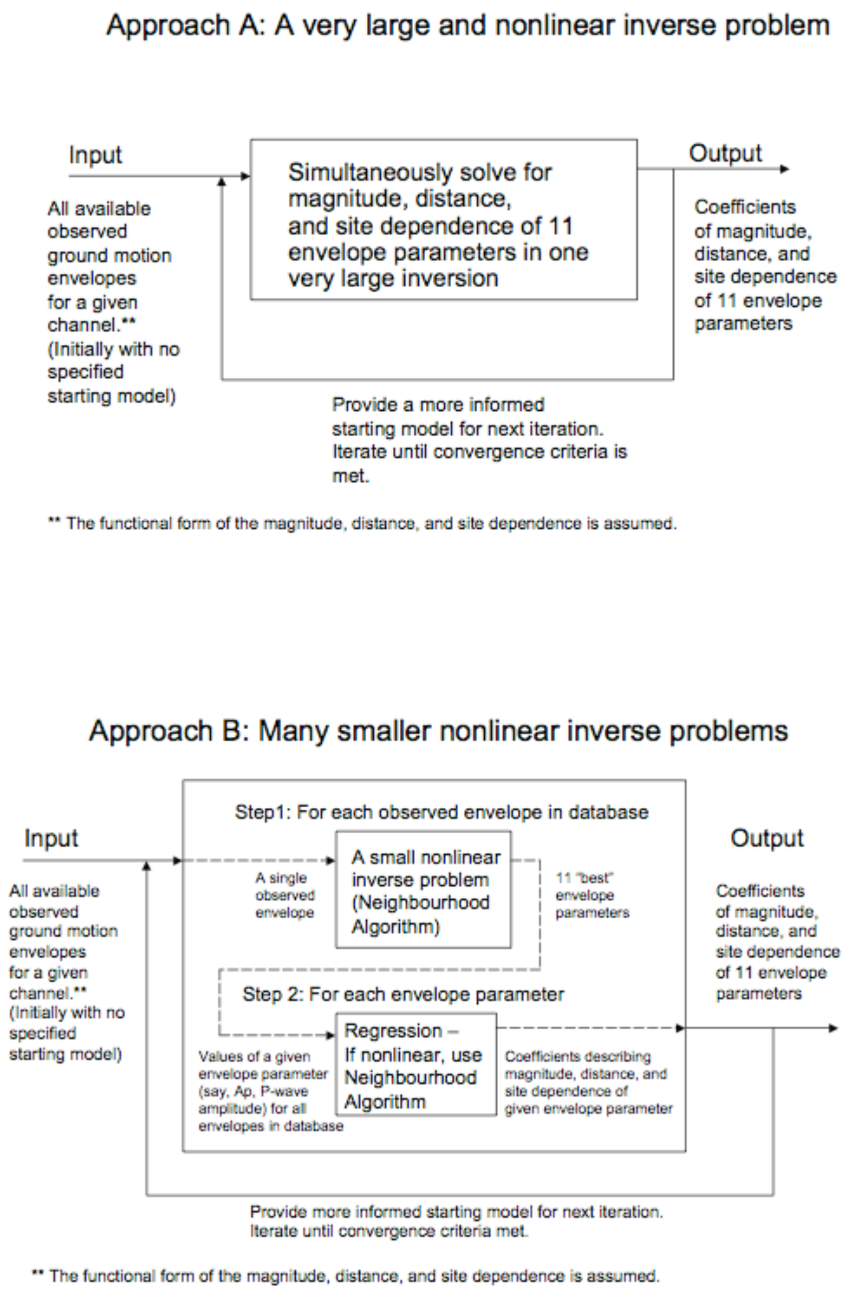


Figure 2: Two possible approaches to characterizing the magnitude and distance dependence of the envelope parameters in Eqn.(2). We adopt Approach B in this study.

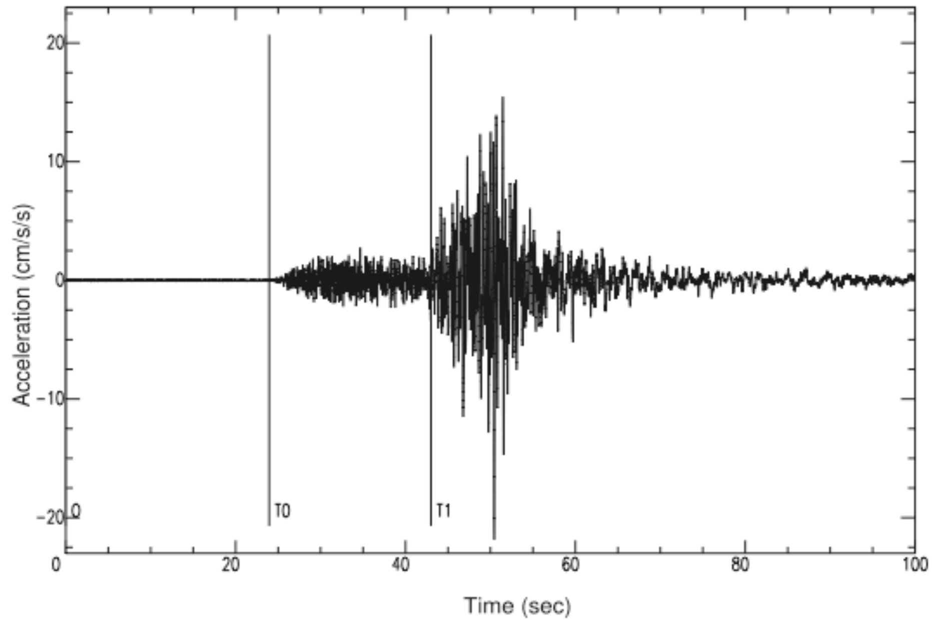


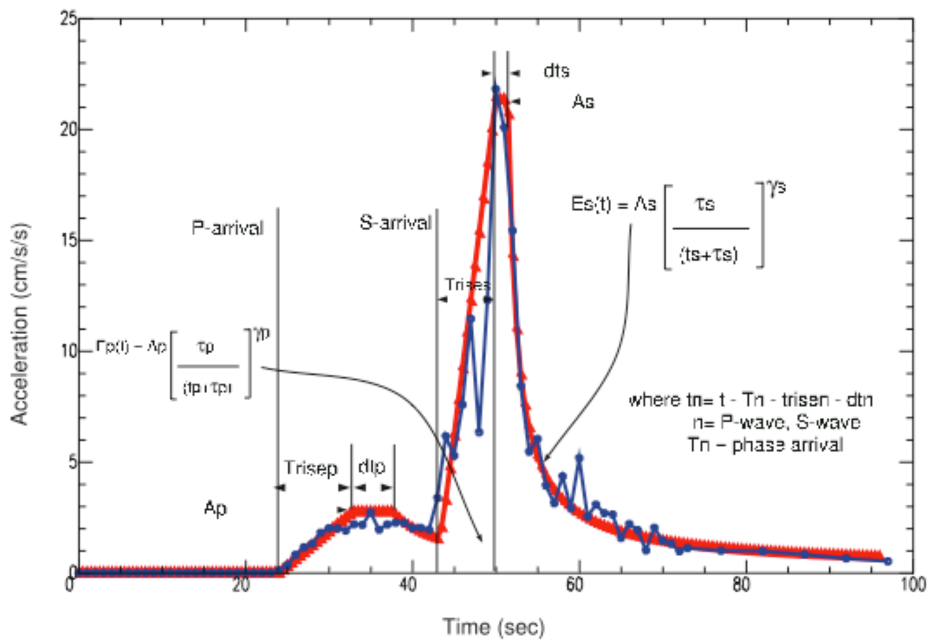


Figure 3: (a) A typical acceleration time history (100 samples per second). (b) The corresponding ground motion envelope, along with the fitted envelope using the neighborhood algorithm to solve for the 11 envelope parameters in Eqn.(2).

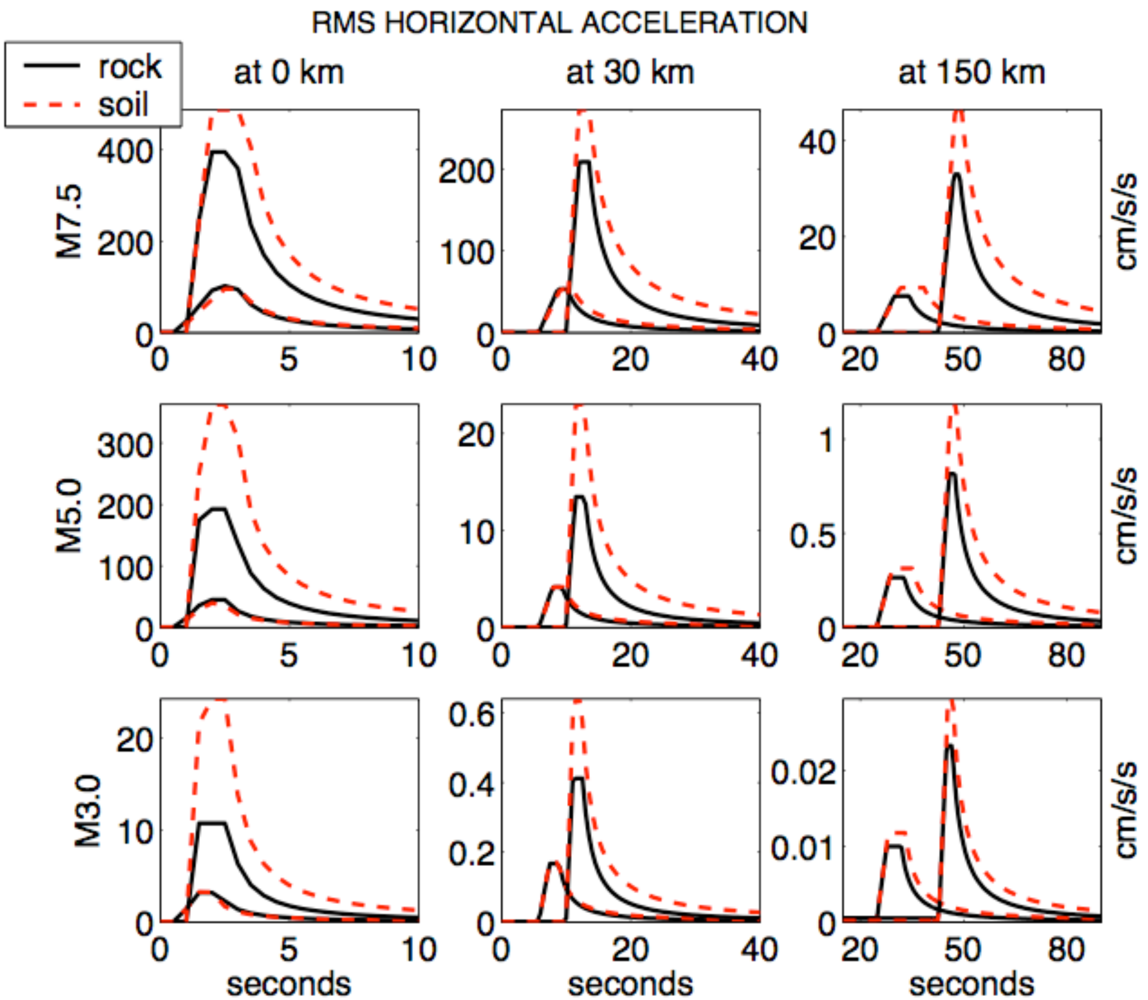


Figure 4: Average horizontal acceleration envelopes on rock and soil sites predicted by the envelope attenuation relationships in Cua (2005) . These are valid for point-source events (up to M6.5).

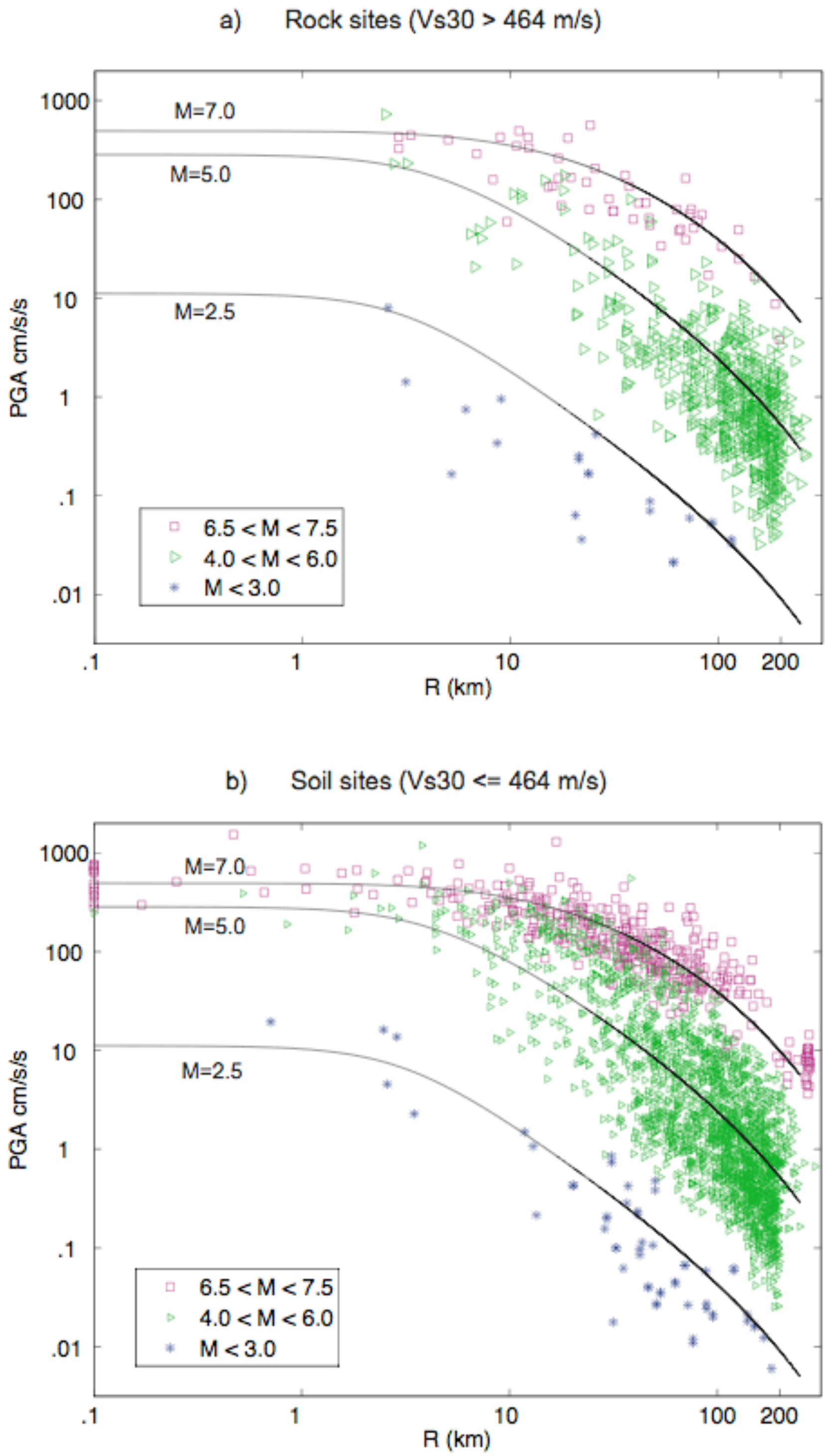


Figure 5: The observed horizontal acceleration amplitudes from the combined NGA and southern California ground motion datasets and the median ground motion levels from the attenuation relationships derived in this study for selected magnitude ranges on (a) rock (Vs30 < 464 m/s), and (b) soil (Vs30 ≤ 464 m/s) sites. *R* is as defined in Eq.2.

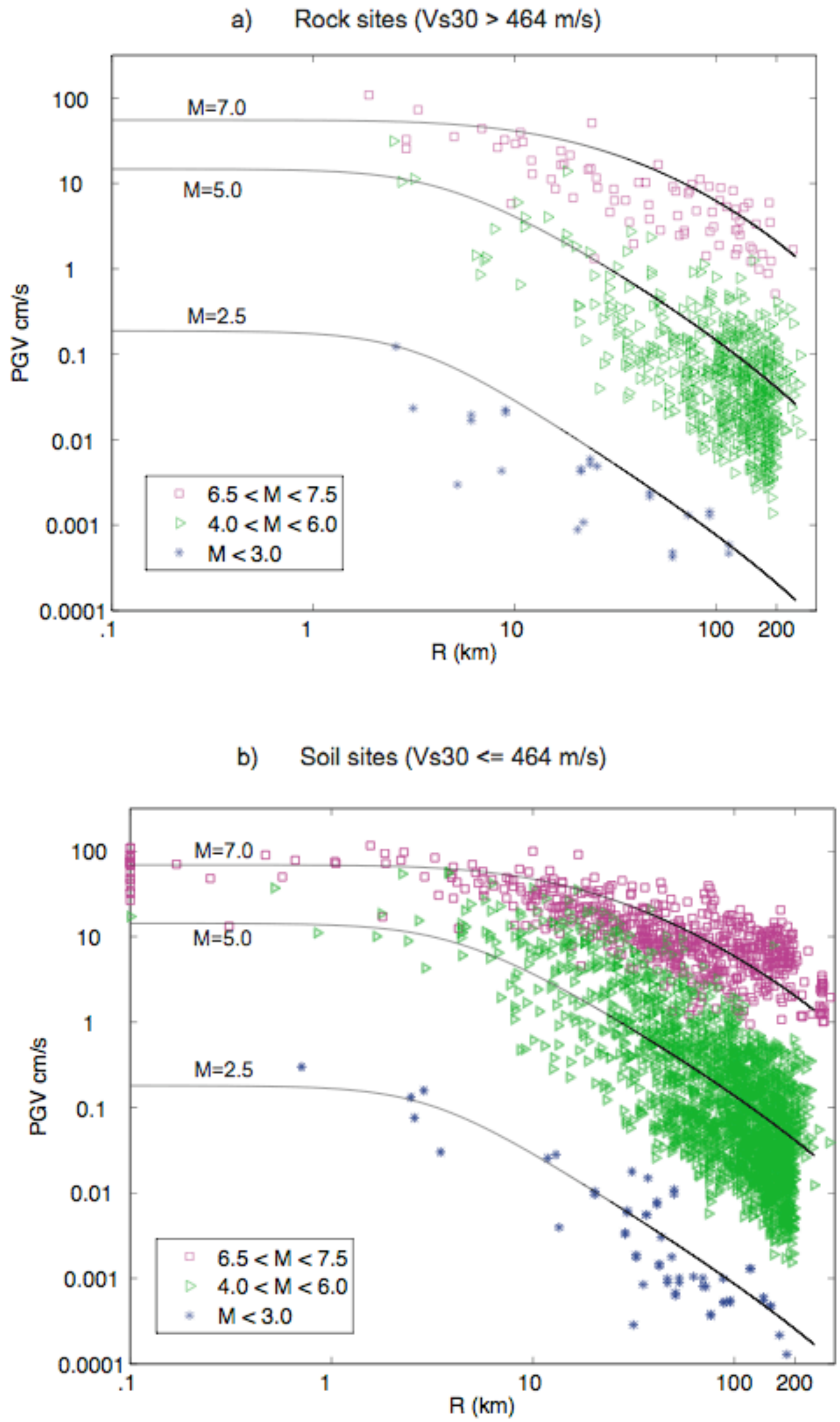


Figure 6: The observed horizontal velocity amplitudes from the combined NGA and southern California ground motion datasets and the median ground motion levels from the attenuation relationships derived in this study for selected magnitude ranges on (a) rock (Vs30 < 464 m/s), and (b) soil (Vs30 ≤ 464 m/s) sites. *R* is as defined in Eq.2.

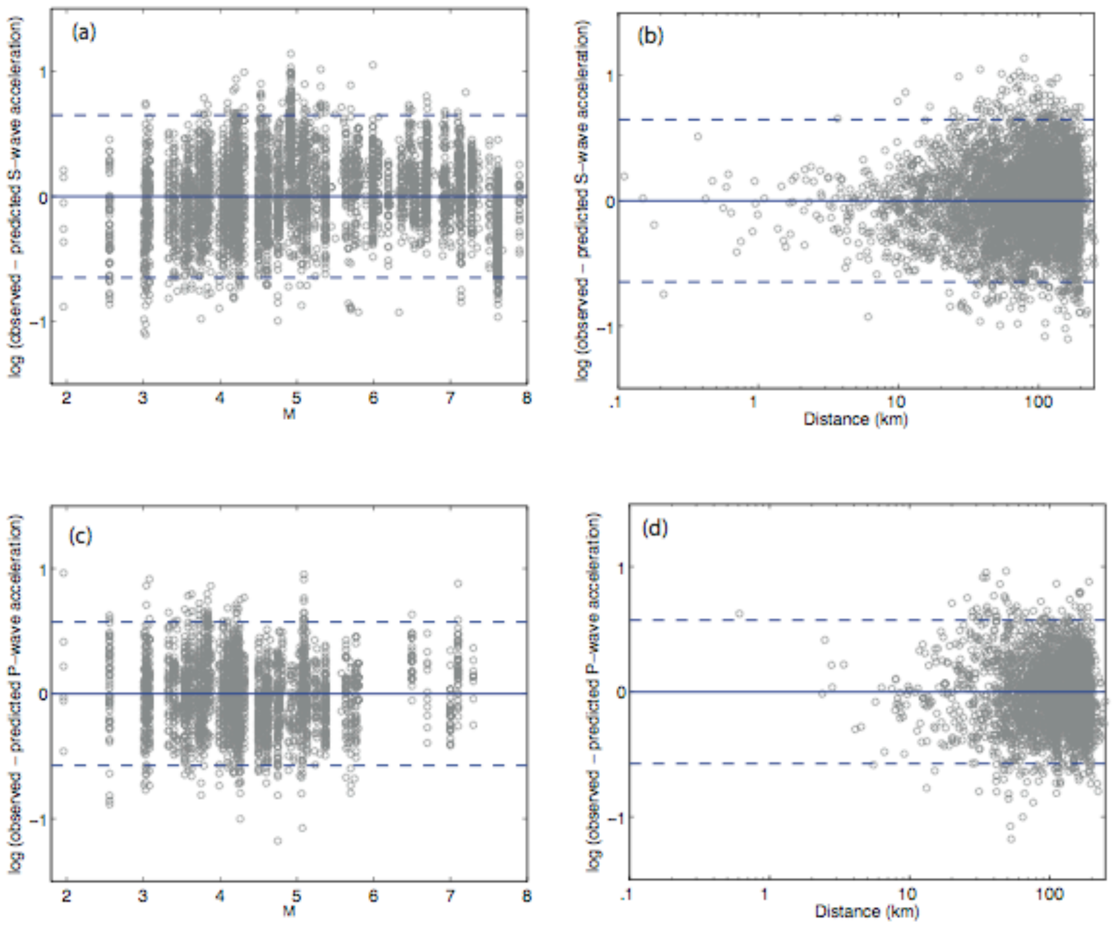


Figure 7: Horizontal S-wave acceleration residuals (combined southern California and NGA dataset) plotted against magnitude (a), and distance (b). Horizontal P-wave acceleration residuals (southern California dataset only) plotted against magnitude (c) and distance (d). The residual plots shown are fairly representative of the general behavior of the residuals for the various channels of ground motion included in this study. There are no obvious trends of the residuals on magnitude or distance.

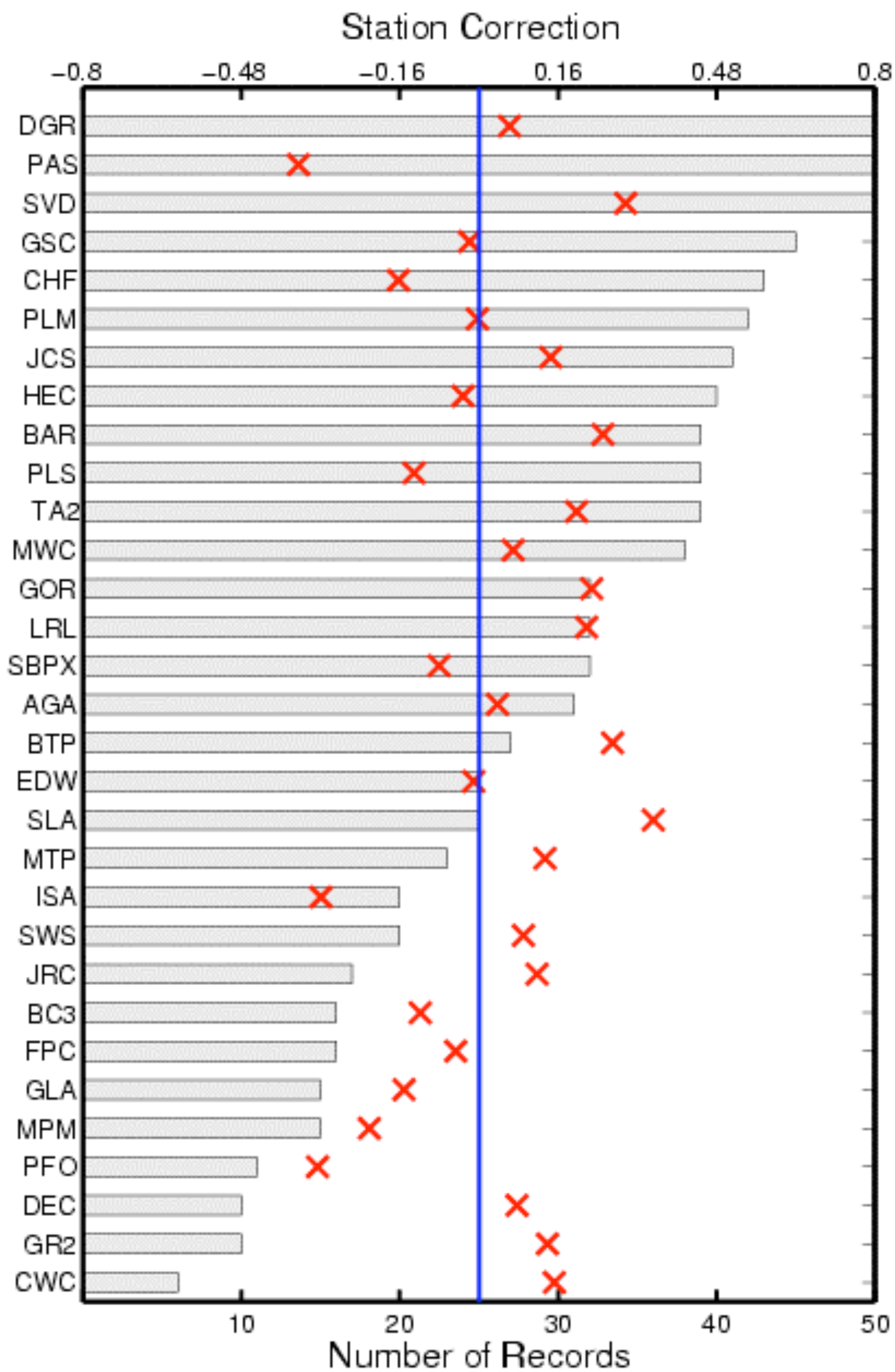


Figure 8: S-wave acceleration stations for SCSN stations on rock sites included in this study. These corrections are calculated relative to the median ground motion level predicted by the S-wave acceleration relationships on rock sites.

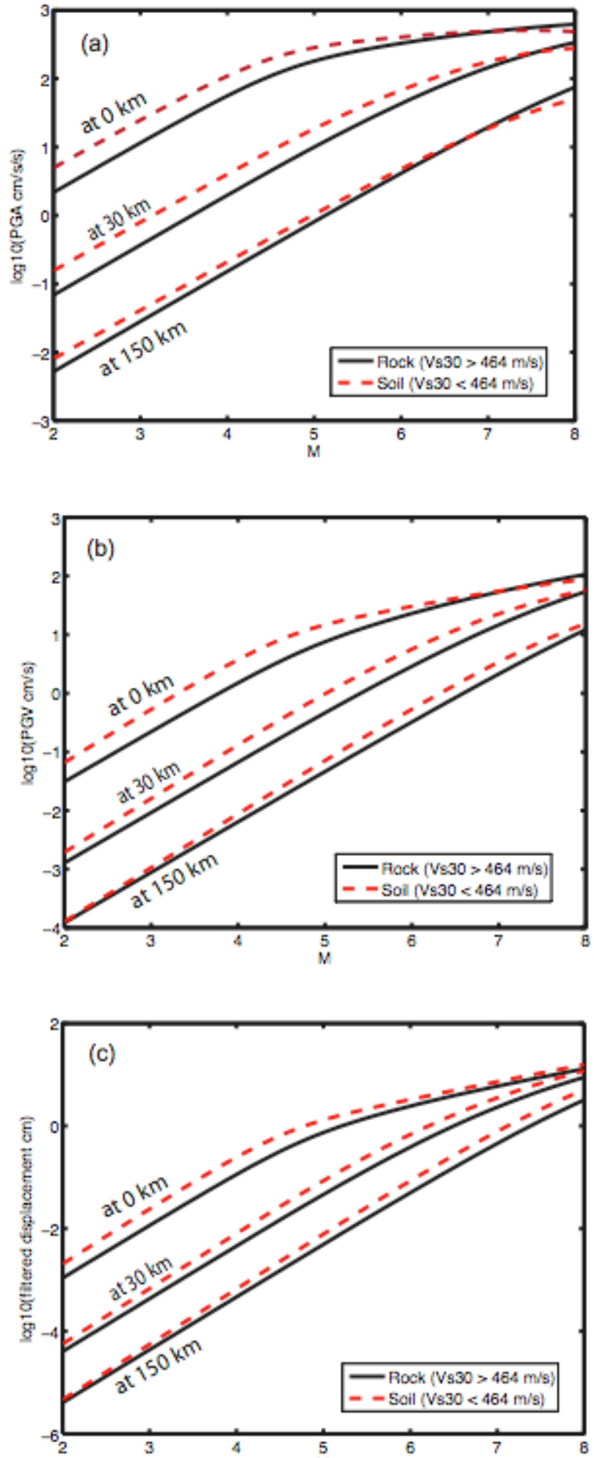


Figure 9: Saturation characteristics as a function of magnitude of (a) PGA, (b) PGV, and (c) peak filtered displacement on rock and soil sites. PGA and PGV relationships are from relationships derived from southern California and NGA data. Displacement relationships are based only on southern California data.

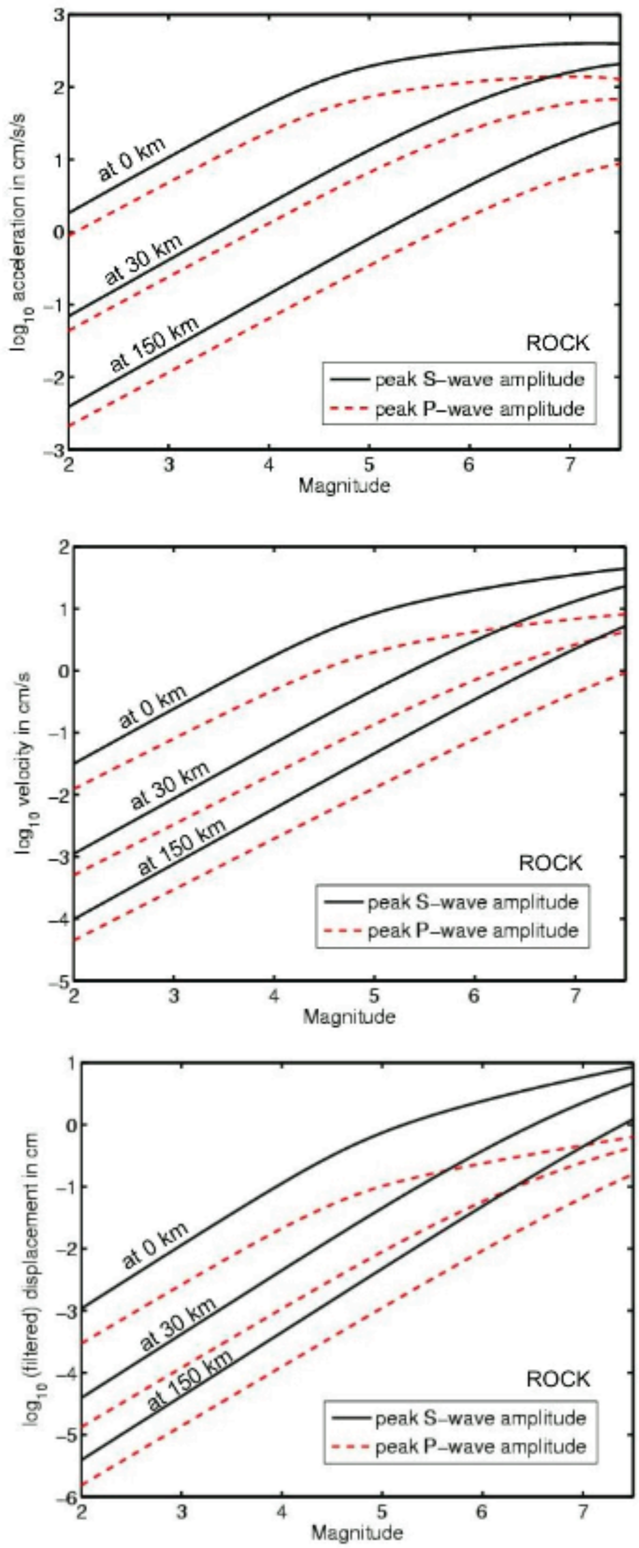


Figure 10: Saturation characteristics of peak P- and S-wave amplitudes (vertical P-wave envelope amplitude and horizontal S-wave envelope amplitude) for various frequency bands.

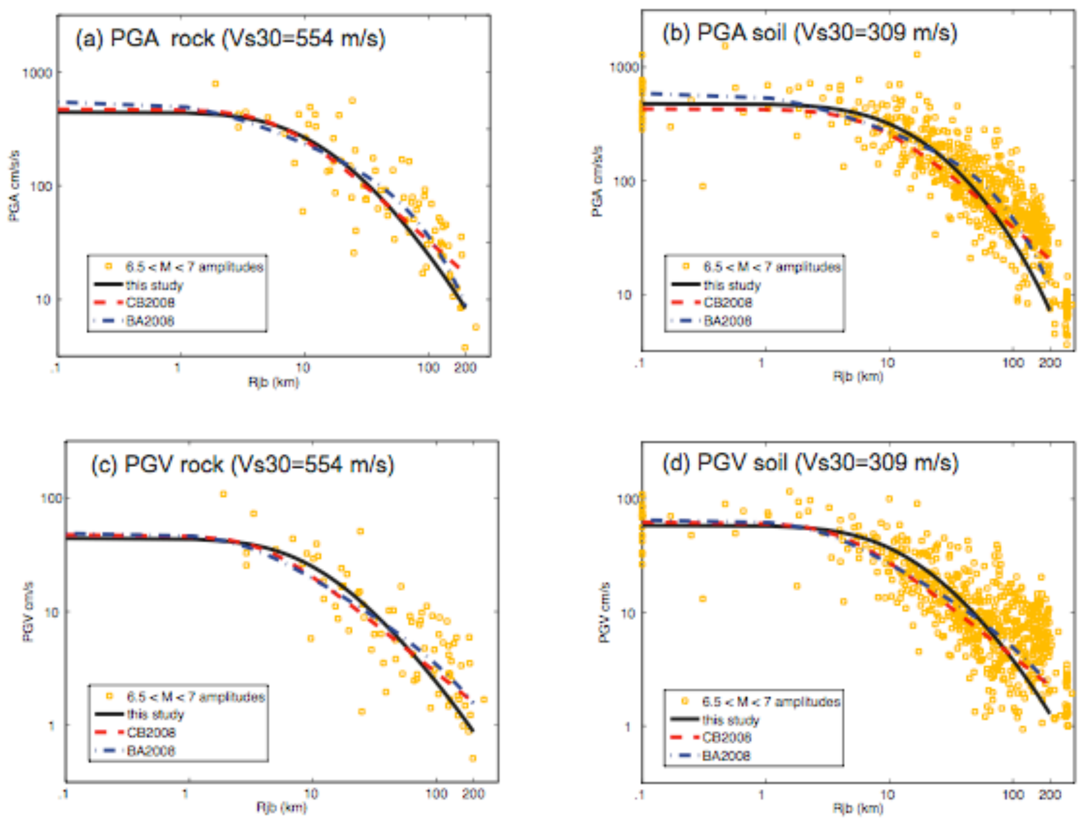


Figure 11: Observed PGA and PGV values from the combined southern California and NGA datasets in the magnitude range 6.5 < M < 7, along with the median M=6.75 ground motion levels from equations developed in this study, Campbell and Bozorgnia (2008), and Boore and Atkinson (2008). The general agreement between the median ground motion levels predicted by the various relationships is expected, since they are all constrained by the same dataset at large magnitudes.

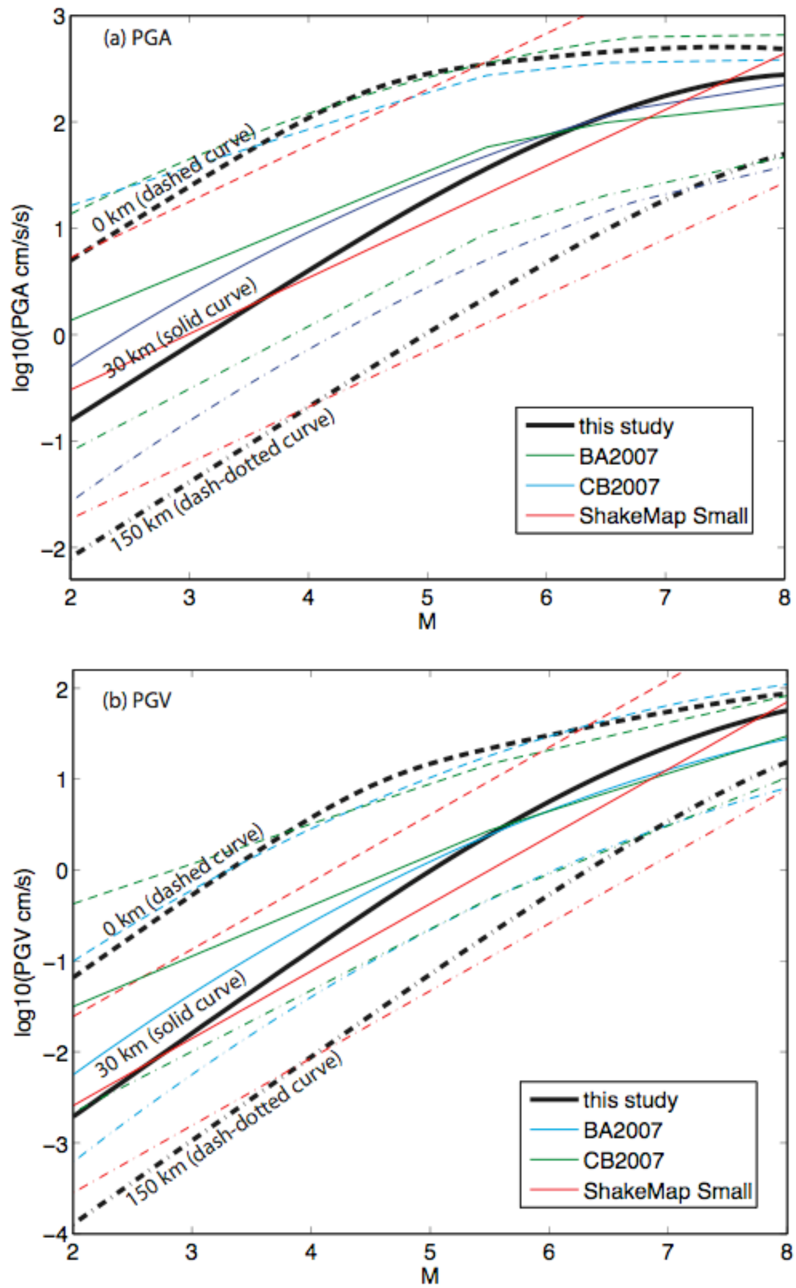


Figure 12: Scaling of (a) PGA and (b) PGV amplitudes at various distances from this study, Boore and Atkinson (2008), Campbell and Bozorgnia (2008), and the ShakeMap Small amplitude relationships (Quitoriano et al, 2003). Our PGA and PGV levels are consistent with Boore and Atkinson (2008) and Campbell and Bozorgnia (2008) at the larger magnitudes, and with the ShakeMap relationship at lower magnitudes. However, the scaling relationships implied by the Boore and Atkinson (2008), Campbell and Bozorgnia (2008), and ShakeMap (2003) relationships cannot be extended beyond the magnitude ranges from which they are derived.

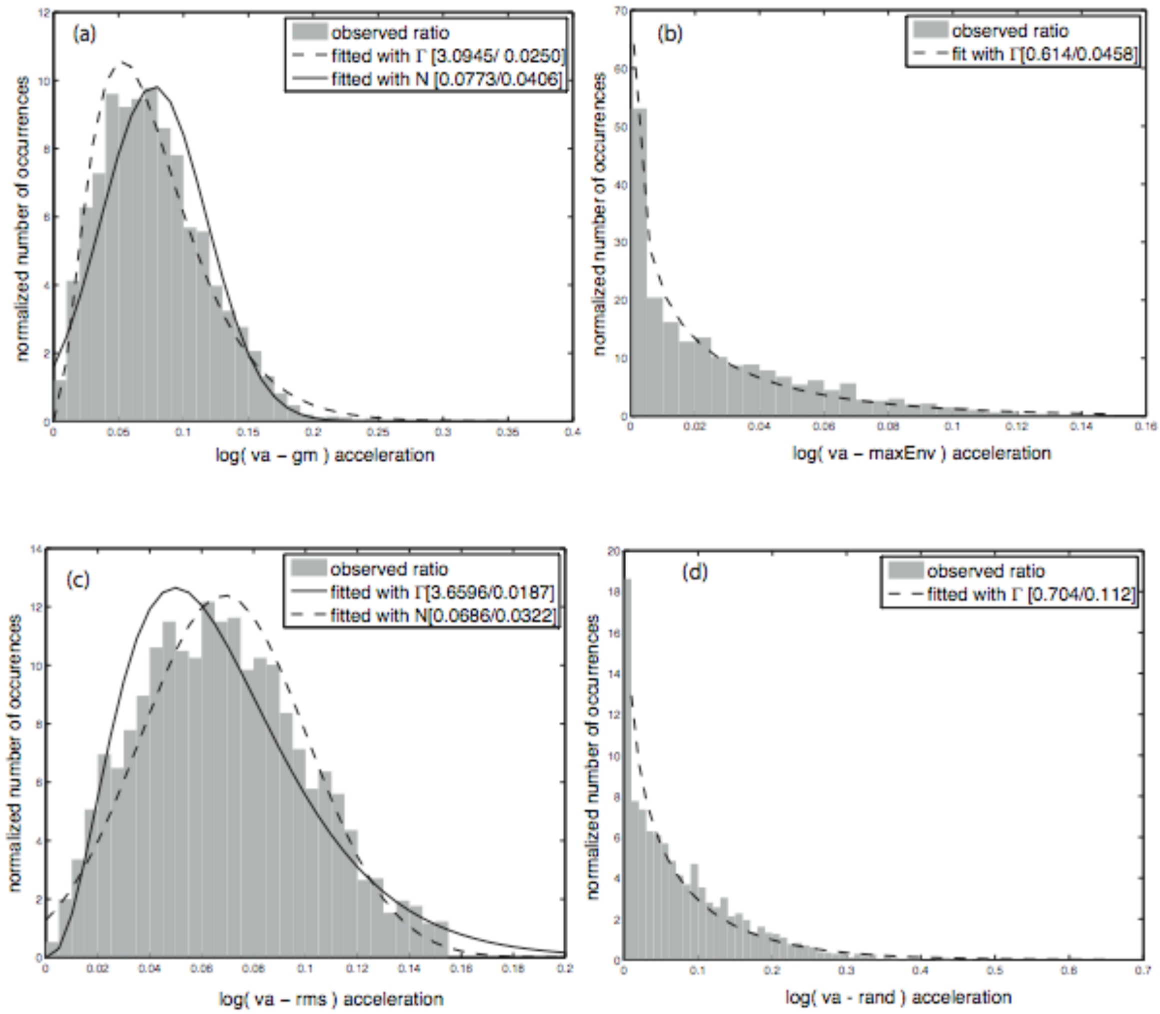


Figure 13: Histograms of the log ratio between different definitions of peak horizontal acceleration.